HYDROTHERMAL SYNTHESIS AND INVESTIGATION OF CATALYTIC ACTIVITIES OF CERIUM OXIDE NANOPARTICLES

A Thesis Submitted to
the Graduate School of Engineering and Sciences of
İzmir Institute of Technology
in Partial Fulfillment of the Requirements for the Degree of

MASTER OF SCIENCE

in Chemistry

by
Mithat BOZ

July 2013
İZMİR

We approve the thesis of **Mithat BOZ**

Examining Committee Members:

_____
Prof. Dr. Serdar ÖZÇELİK
Department of Chemistry, İzmir Institute of Technology

_____
Prof. Dr. Selahattin YILMAZ
Department of Chemical Engineering, İzmir Institute of Technology

_____
Assoc. Prof. Dr. Mehtap EMİRDAĞ EANES
Department of Chemistry, İzmir Institute of Technology

_____
Assoc. Prof. Dr. Ali ÇAĞIR
Department of Chemistry, İzmir Institute of Technology

_____
Assist. Prof. Dr. Mustafa EMRULLAHOĞLU
Department of Chemistry, İzmir Institute of Technology

19 July 2013

_____
Assoc. Prof. Dr. Mehtap EMİRDAĞ EANES
Supervisor, Department of Chemistry, Institute of Technology

_____
Assoc. Prof. Dr. Ali ÇAĞIR
Co-supervisor, Department of İzmir Chemistry, İzmir Institute of Technology

_____
Prof. Dr. Ahmet EROĞLU
Head of the Department of Chemistry

_____
Prof. Dr. R. Tuğrul SENGER
Dean of the Graduate School of Engineering and Sciences

ACKNOWLEDGEMENTS

In this study there are too many people to be thanked yet first of all my superb supervisor Assoc. Prof. Mehtap EMİRDAG EANES who has supported me throughout my thesis and appreciated me even for simple things. Whenever I had a problem, she always gave me her valuable advices. One simply could not wish for a better or friendlier supervisor.

Also, I would like to thank my co-supervisor Assist. Prof. Dr. Ali Çağır for his kind support, his guidance and valuable comments.

Next, I want to thank Clemson University of Materials Research for Transmission Electron Microscope images, Center (IYTE MAM) for Scanning Electron Microscope and X-ray Diffraction analysis and Pınar BAYDARA for GC-MS analysis.

For all their supports, thanks to my friends in IZTECH especially Taylan MEŞİN, Banu ÖNEN, Özlem ECE, Muhammed ÜÇÜNCÜ, Erman KARAKUŞ, İsmail AKÇOK, Esen DÖNERTAŞ, Merve DEMİRKURT, Seçil SEVİM, Melih KUŞ, Fırat ZİYANAK and Doğan TAÇ.

Finally, my deepest gratitude goes to my lovely family, they are always there for me. Their support, motivation, positive criticism and endless love gave me huge power to reach success in this thesis and also in my life.

ABSTRACT

HYDROTHERMAL SYNTHESIS AND INVESTIGATION OF CATALYTIC ACTIVITIES OF CERIUM OXIDE NANOPARTICLES

Single crystalline cerium oxide nanoparticles were synthesized with hydrothermal method by mixing cerium nitrate [$Ce(NO_3)_3.6H_2O$] aqueous solution with NaOH and urea. SEM, TEM and XRD characterization methods were used in order to identify morphology.

First part of the study includes the work on effect of hydrothermal parameters, such as base type and concentration, surfactant, reaction temperature, and time on particle size and morphology. The reaction time, temperature and concentration trials were carried out for urea only. When base types were compared, smaller particles were synthesized in the presence of NaOH yet smaller crystalline sized particles were obtained in the presence of urea. Effect of surfactant was investigated however there was no significant effect on size or morphology. Effect of concentration was clear, cubic and triangular prism shaped particles obtained for concentrations lower than 1M, and for concentration higher than 1M, agglomerated spherical particles were obtained. Reaction time and temperature were also investigated and all the reactions resulted in agglomerated non-uniform spherical particles. There was no considerable difference in particle and crystalline size for these samples. Due to the sub-micron size of CeO_2 synthesized using urea, CeO_2 nanoparticles synthesized using NaOH for catalysis.

Second part includes the investigation of catalytic property of CeO_2 nanoparticles. CeO_2 nanoparticles were used as catalyst in the synthesis of flavone from 2'-hydroxychalcone. Total flavone yield was approximately 42.5 %. Several reaction parameters were studied in order to achieve the flavone synthesis. TLC, GC-MS and NMR were used in order to monitor the results of the reactions.

ÖZET

SERYUM OKSİT NANOPARÇACIKLARININ HİDROTERMAL SENTEZİ VE KATALİTİK ETKİSİNİN İNCELENMESİ

Tek kristal seryum oksit nanoparçacıkları seryum nitratın [$Ce(NO_3)_3.6H_2O$] NaOH ve üre ile sulu çözeltilerinin hazırlanmasının ardından hidrotermal metot ile sentezlenmiştir. Taramalı ve geçirimli elektron mikroskopu ve X-ray kırınımı yöntemleri kullanılarak parçacıkların morfoloji ve kristal özellikleri saptanmıştır.

Çalışmanın ilk kısmı reaksiyon zamanı, reaksiyon sıcaklığı, polimer, baz çeşidi ve konsantrasyonu gibi parametrelerin değişiminin parçacık boyutuna ve morfolojisine olan etkilerini içermektedir. Reaksiyon zamanı ve sıcaklığı ve baz konsantrasyonu denemelerinde sadece üre kullanılmıştır. Baz tipleri karşılaştırıldığında, NaOH ile daha küçük parçacık boyutuna ulaşılırken, üre ile daha küçük kristal boyutuna ulaşılmıştır. Polimer etkisi de incelenmiş olup, parçacığın boyut ve morfolojisini değiştiren net bir etkiye rastlanmamıştır. Baz konsantrasyonundaki değişimde ise 1M'dan küçük konsantrasyonlarda kübik ve üçgen prizma şeklinde, 1M'dan büyük konsantrasyonlarda ise topaklanmış küre biçimdeki parçacıklar elde edilmiştir. Reaksiyon zamanı ve sıcaklığının etkileri de araştırılmış, bütün denemelerde topaklanmış düzgün olmayan küre biçiminde parçacıklar gözlemlenmiştir. Bu örnekler için parçacık boyutu ve kristal boyutunda dikkate değer bir fark görülmemiştir. Üre ile sentezlenen parçacıkların mikron altı boyutlarda olmasından dolayı organik reaksiyonlarda NaOH ile sentezlenen CeO_2 nanoparçacıkları katalizör olarak kullanılmıştır.

İkinci kısımda ise CeO_2 nanoparçacıklarının katalitik özellikleri araştırılmıştır. CeO_2 nanoparçacıkları 2'-hidroksiçalkondan flavon dönüşümünde katalizör olarak kullanılmıştır. Reaksiyonların sonucunda, toplam 42.5 % oranında dönüşüm saptanmıştır. Ayrıca değişik reaksiyon parametrelerinin flavon dönüşümü üzere olan etkileri de araştırılmıştır. Sonuçlar TLC, GC-MS ve NMR ile takip edilmiştir.

TABLE OF CONTENTS

LIST OF FIGURES

Figure **Page**

LIST OF TABLES

Table **Page**

CHAPTER 1

INTRODUCTION

Nanotechnology is a field, deals with every branch of science such as biology, chemistry, physics and enginering subjects. In general its main definition is known as the design, characterization, production, and application of structures, devices, and systems by controlled manipulation of size and shape at the nanometer scale (atomic, molecular, and macromolecular scale) that produces structures, devices, and systems with at least one novel/superior characteristic or property.

The fabrication of nanomaterials is based on two methods; top-down and bottom-up methods. Briefly in top-down method starting, nano scale materials are formed by processing of bulk materials. It includes various techniques like thermal, chemical, high energy and mechanical. According to these techniques thermal methods, lithographic methods, high energy methods can be given as example for top-down methods.

In bottom-up method, atoms and molecules are used in order to form larger nano materials compare to themselves. Self-assembly is an important factor for bottom-up method and bottom-up liquid phase methods are best methods for self-assembled systems. Like in top-down method, in bottom-up method several techniques are used; atomic layer deposition, chemical vapor deposition, metal-organic chemical vapor deposition. Liquid phase methods, chemical vapor deposition methods, electrodeposition methods, atomic layer deposition methods are some of the examples for bottom-up methods.

Quantum effect is a new term that has gained importance with nanotechnology. When the size of particle reachs to nano scale different and often enhanced proporties of matter are observed. One of them is the high volume to surface ratio and the other one is some change on the physical properties of matters compare to their bulk forms (Quantum effect). The relationship between surface area and particle size is inversially proportional with each other. As particle size decreases the surface to volume ratio increases. The relation can be seen in Figure 1.1.

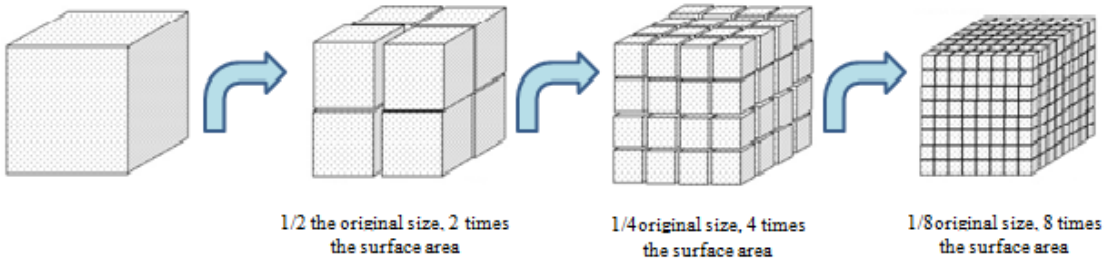

Figure 1.1. Particle size-surface area relationship

Higher surface area which can be reached by lowering the particle size to nano scale is so important especially for catalytic processes yet this high surface area proportional with high surface energy and that makes nanoparticles thermodynamically unstable. For more stable particles there are some methods that gather small particles to form larger ones in order to decrease surface energy. Ostwald ripening process and sintering process are some methods used for this situtation. Ostwald ripening can be defined as dissolution of small crystals and the redeposition of the dissolved species on the surfaces of larger crystals (Ostwald 1896). An everyday example of Ostwald ripening is the re-crystallization of water within ice cream which gives old ice cream a gritty, crunchy texture. Larger ice crystals grow at the expense of smaller ones within the ice cream, creating a coarser texture (Clark and Chris, 2004). In sintering process small particles, generally powder, gather to form large particles. Sintering is based on atomic diffusion so it is needded high temperature. This requirement is the main difference between Ostwald ripening and sintering (Kang 2005).

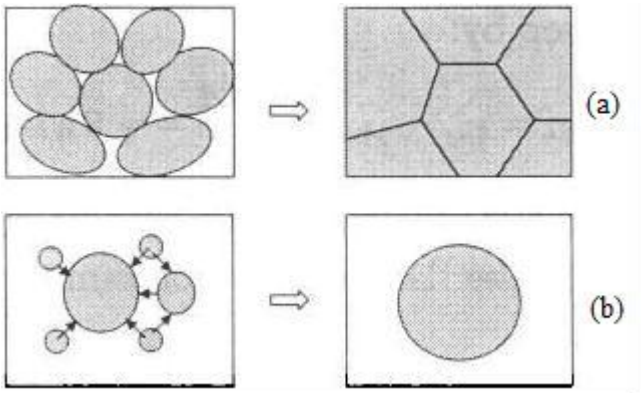

Figure 1.2. Illustration of sintering (a) and Ostwald process (b)
(Source: Cao 2004)

1.1. Cerium Oxide Nanoparticles

Because of the rising importance to nanomaterials everyday, there are too many studies on this subject. According to that some groups have certain advantages for some topics like rare earth oxides. Rare earth oxide nano-particles have exceptional luminescence, magnetic and electronic properties due to their unfilled 4f electronic structure. As such, rare earth-based phosphors, magnetic materials, hydrogen storage material and high surface area support catalyst are being widely developed (Tok, et al. 2007). Cerium oxide (CeO_2), which is one of the rare earth oxides, nanoparticles have been extensively studied over the last two decades. Cerium oxide, also known as cerium dioxide and ceria, has pale yellow color as shown in Figure 1.3.

Figure 1.3. Cerium oxide powder

Pure CeO_2 has a fluorite structure, shown in Figure 1.4, space group F m3m. The lattice is commonly described as a ccp array of cerium ions, with oxygen ions occupying all the tetrahedral holes. Each cerium cation is coordinated by 8 oxygen anions at the corner of a cube. If the structure is extended and we view a cell with oxygen at the corners of a cube (Figure 1.4 b,c), we see that alternate cube centers are empty or occupied by a cerium ion. This structure results in significant “holes” in the lattice, which contributes to the ease with which oxygen moves through the structure.

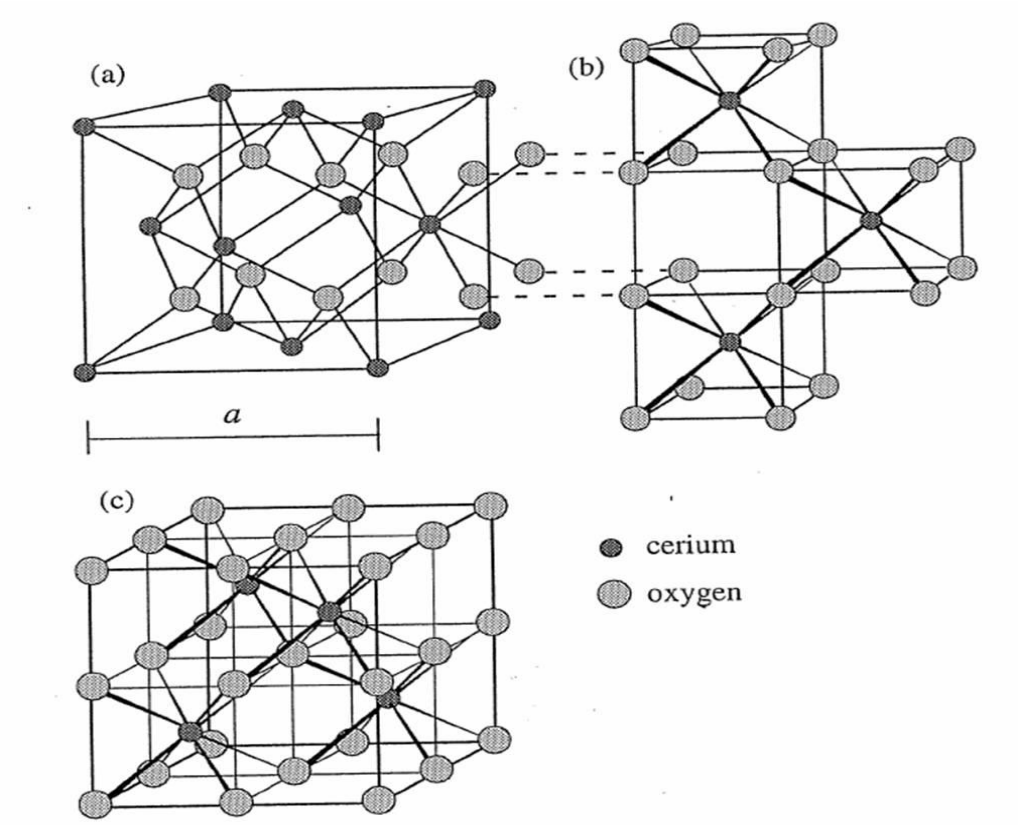

Figure 1.4. Crystal structure of cerium oxide (a) unit cell as a *ccp* array of cerium atoms and (b) and (c) the same structure redrawn as a primitive cubic array of oxygen ions. (Source: Trovarelli 2002)

Cerium's electron configuration is $4f^{1}5d^{1}6s^{2}$. It is the first element in the periodic table with partially occupied f orbitals, and stable oxides exist for +3 and +4 valency. A study of the quantum behavior of ceria indicates that the electron in the f orbital becomes localized to the cerium atom upon creation of an oxygen vacancy. Subsequently, the electrons again become delocalized to another oxygen. In this way, the reduction process can be thought of as formation, migration and ordering of Ce^{3+}-vacancy complexes. Depending on the partial pressure of oxygen in the environment, ceria will form a range of oxides CeO_x. Interestingly, for values of $1.714 < x < 2$, the lattice retains the fluorite structure; the oxygen ions move through the lattice, forming ordered vacancies, and the cerium cations remain in the same position within the lattice. The lattice volume changes, however, as the Ce^{3+} Radius (1.14°A) is larger than the Ce^{4+} radius (0.97°A).

1.2. Applications of Cerium Oxide Nanoparticles

Because of its unique properties, especially for oxygen stroge capacity (OSC) there is a wide range of applications of ceria nanoparticles. It is generally used as gas sensors(Jasinski, et al. 2003), catalysts(Bera,et al. 2003), ultraviolet absorbers(Li, et al. 2002), polishing materials(Shchukin and Carusa 2004), optical devices(Goubin, et al. 2004), hydrogen stroge materials(Sohlberg, et al. 2001) and fuel cells(Jacobs, et al. 2003). In literature, there are many studies on cataylitic properties of cerium oxides. Wang, et al. compared the catalytic activies of cerium oxides and other oxides nanoparticles on incineration of aromatic compounds (Wang, et al. 2004).Zou, et al. compared the catalytic activities of different ratio of cerium-manganase binary oxides on incineration of carbon monoxide and toulene (Zou, et al. 2010).

1.3. Chalcones

A group of compounds having different substitution patterns on the two aromatic rings of 1,3-diphenyl-2-propen-1-one which is known as chalcone **(1)** and it is linked by a three carbon α,β-unsaturated carbonyl system. It is an important class of natural product and subclass of the flavonoid family which have been reported a wide spectrum of biological activities including anti-inflammatory, anti-mutagenic, anti-bacterial and anti-fungal (Dimmock, et al. 1999) (Go and Lui 2005) (Nowakowska and Kedzi 2008). Some of the derivatives of chalcone are used as drugs, sunscreen agents and aqueous sweeteners (Li, et al. 2002) (Karthikeyan, et al. 2007) .

For the synthesis of chalcone, aldol condensation and Claisen-Schmidt condensation are mostly used strategies (Kerher, et al. 2003) (Yarishkin 2008) . Acid catalyzed and base catalyzed methods are used widely for chalcone synthesis. While dry HCl, titanium trichloride ($TiCl_3$), aluminium trichloride (Al_2Cl_3) and ruthenium trichloride ($RuCl_3$) are used in acid catalyzed method, sodium hydroxide (NaOH), lithium hydroxide (LiOH), potassium hydroxide (KOH) and barium hydroxide ($Ba(OH)_2$) are used in base catalyzed (Anderson 2001) .

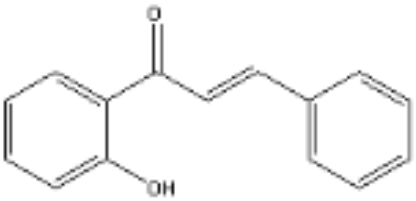

1

Figure 1.5. Structure of 2’-hydroxychalcone

1.4. Flavanones

Flavanones **(2)** are one of the subclass of flavanoids. The transformations of 2’-hydroxychalcones **(1)** to flavanone **(2)** by chalcone-flavanone isomerase enzyme in vivo. Flavanones can also be synthesized by Micheal addition type cyclization of 2’-hydroxychalcones **(1)** in vitro as shown in Figure 1.6.

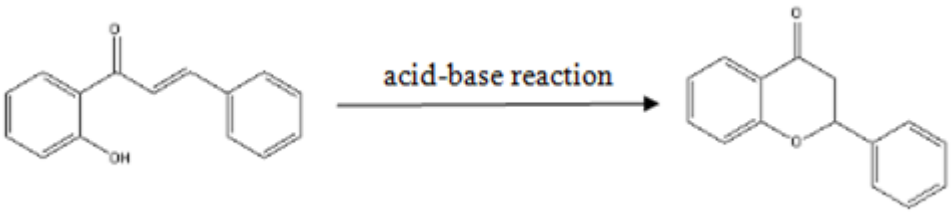

Figure 1.6. Michael addition type cyclization of 2’-hydroxychalcone (1)

Like other flavanoids, they also have biological activities such as anti-oxidant, anti-bacterial, anti-cancer (Havsteen, 2002).

Cyclization reaction of 2’-hydroxychalcone can be done under both acidic and basic catalyst. Transformation of 2’-hydroxychalcone **(1)** to flavanone **(2)** by refluxing in glacial acetic acid is an example of acid catalized cyclization method (Cabrera, et al. 2007).

1.5. Flavones

Flavones (**3**) represent one of the largest subgroups within the flavonoids (Figure 1.7). FNS I and FNS II, two independently evolved and mechanistically different

enzymes, can convert the flavanones into flavones (Martens and Mithöfer, 2005). Also there are some synthetic methods for flovane synthesis: Algar-Flynn-Oyamada reaction (Gormleg, et al 1973), Allan-Robinson reaction (Dyke, et al. 1961) and Auwers synthesis (Auwers 1908).

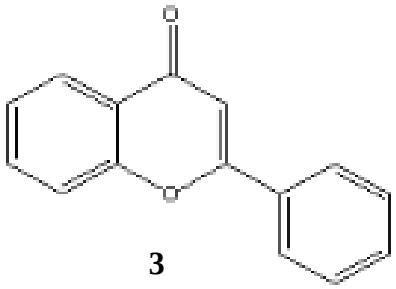

3

Figure 1.7. Structure of flavone.

Epidemiology and animal studies suggested that a high dietary intake of flavonoids, including flavones, may be linked to a reduced risk of several cancers (e.g., lung and colon cancer), coronary heart disease, chronic inflammation, and osteoporosis (Middleton et al., 2000; Kromhout, 2001; Tabak et al., 2001; Ross and Kansum, 2002; Manach et al., 2003; Arts and Hollman, 2005). Flavones themselves have biochemical and pharmacological activities which are beneficial for human health, including antioxidant, anticancerogenic, anti-inflammatory, antiproliferative, antiangiogenic, and antiestrogenic effects, and ingestion produces no or very little toxicity (Havsteen, 2002).

1.6. Synthesis Methods

Ceria nanoparticles can be synthesized by many different methods. Mostly used ones are sol-gel, sonochemistry, chemical precipitation, microemlsion, solvothermal and hydrothermal methods. Ganguli, et al. (2008) synthesized ceria nanoparticles about 10 nm by microemulsion method. Zhang, et al. (2007) synthesized cerium oxide nanorods in ultrasonicator by sonochemical method. Gu and Soucek (2007) prepared cerium oxide nanoparticles via the sol-gel route from aqueous solutions of inorganica precursor. Zawadzki (2008) synthesized ceria nanoparticles from cerium nitrate in diethylene and hexamine solutions by solvothermal method. Tunusoğlu, et al.(2012)

produced ceria nanoparticles smaller than 10 nm by chemical precipitation method. Tok, et al. (2007) synthesized cerium nanoparticles by low temperature hydrothermal method.

1.6.1. Sol-gel Synthesis

Sol-gel method is occupied an important place for fabrication of nanomateials. Sol-gel processing is a wet chemical synthesis approach that can be used to generate nanoparticles by gelation, precipitation, and hydrothermal treatment. Sol (solvent) is a suspension or a colloidal solution that acts as a precursor for an integrated network (or gel). The first step is prepared the sol, after that it is polimerized and forms a wet gel. Finally this wet gel is dried by heating properly to prevent the solvent. Figure 1.8 shows the schematic route of sol-gel process.

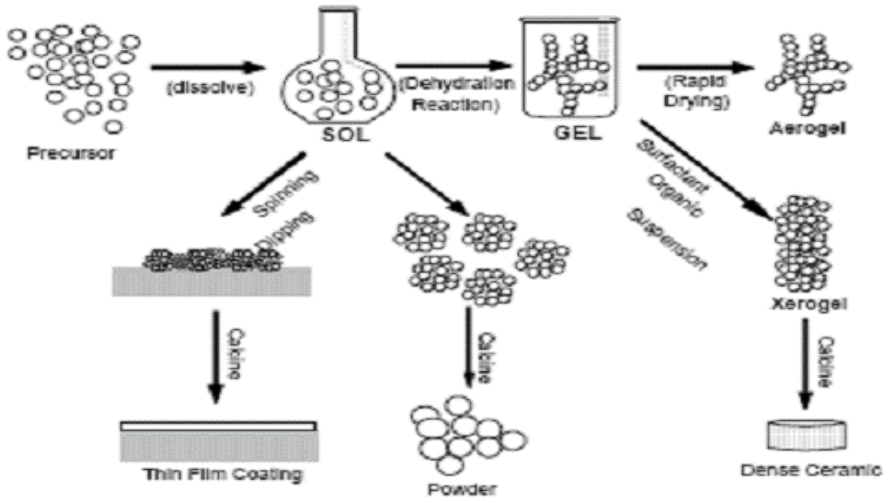

Figure 1.8. Sol-gel processing options.

Metal alkoxides and metal salts (chlorides, nitrates) are generally used as starting precursor for sol-gel method.

1.6.2. Microemulsion Method (Reverse Micelles)

Microemulsions are used for synthesis of various types of nanoparticles. By controlling the very low interfacial tension (~10^{-3} mN/m) through the addition of a co-surfactant, these microemulsions are produced spontaneously without the need for significant mechanical agitation (Higgins 1997).

Microemulsions are homogeneous, macroscopically, isotropic and thermodynamically stable solutions containing at least three components, namely a nonpolar phase (generally oil), a polar phase (generally water) and a surfactant. On a microscopic level the surfactant molecules form an interfacial film separating the polar and the non-polar domains. Different microstructures are formed by interfacial layer that ranging from droplets of oil dispersed in a continuous water phase (O/W-microemulsion) over a bicontinuous ‘‘sponge’’ phase to water droplets dispersed in a continuous oil phase (W/O – microemulsion) (Julian, et al. 2006) (Destree, et al. 2008) (Zhong-min, et al. 2007) (Wanzhong, et al. 2006).

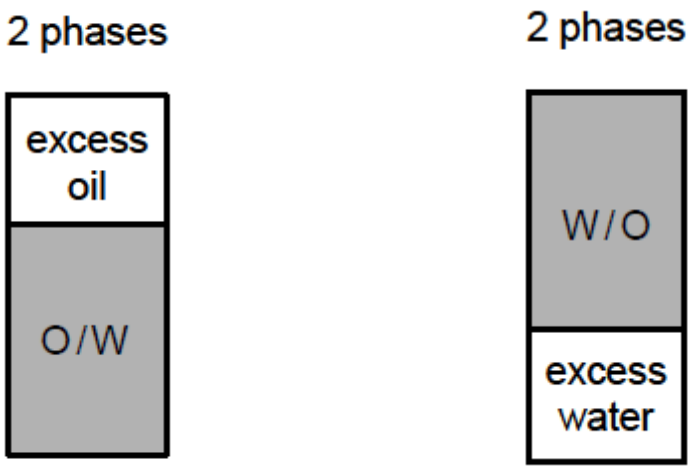

Figure 1.9. Microemulsion types.
(Source: Winsor 1948)

Reverse micelles are surfactant molecules that dissolved in organic solvents to form spheroidal aggregates (Pileni 1989). Figure1.10 shows a typical structure of reverse micelle.

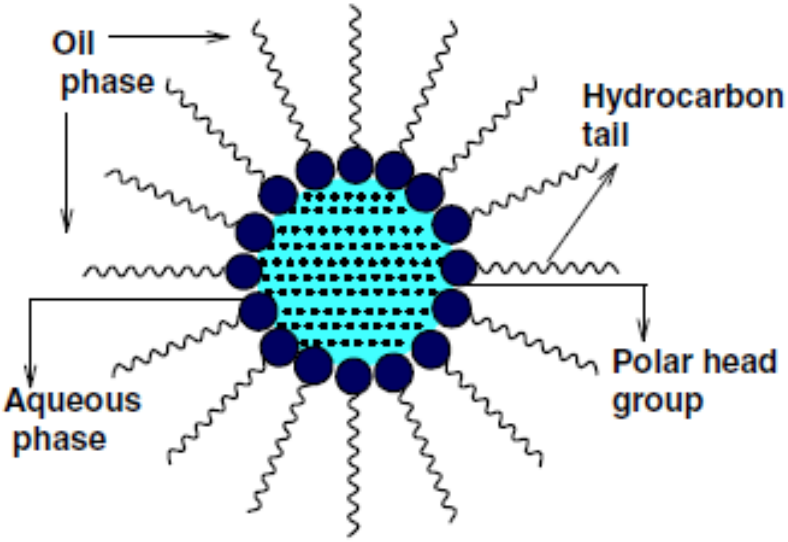

Figure 1.10. Structure of reverse micelle.

Nanoparticles of metal oxides are usually produced by the hydrolysis method in which metal alkoxide react with water droplets in the reverse micelles. Nanoparticles of metal oxides such as ZrO_2, TiO_2, SiO_2, GeO_2 and Fe_2O_3 have been synthesized. (Chang, et al. 1994) (Esquena, et al. 1997) (Lopez-Perez, et al. 1997) (Chen, et al. 2008)

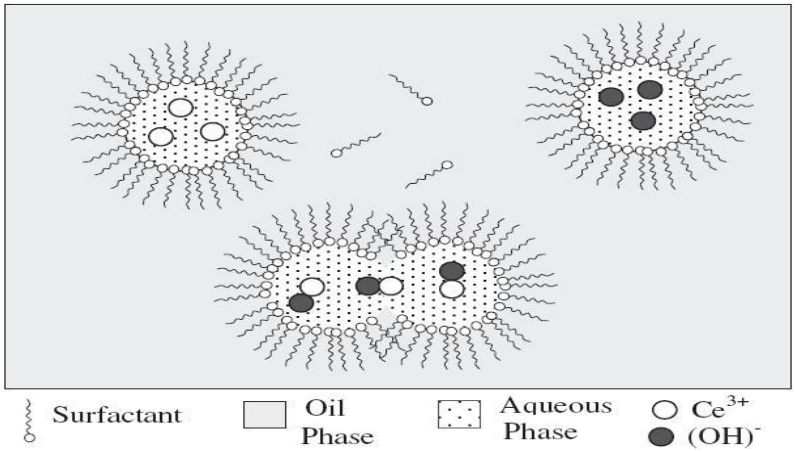

Figure 1.11. Illustration of nanoparticle synthesis using reverse micellar synthesis. (Source: Sathyamurthy 2005)

1.6.3. Sonochemistry Method

In sonochemistry, an acoustic cavitation process can generate a transient localized hot zone with extremely high temperature gradient and pressure. Such sudden changes in temperature and pressure assist the destruction of the precursor and the formation of nanoparticles (Suslick, et al. 1996).

Recently, CeO_2 nanoparticles and nanotubes prepared by ultrasonication have been reported (Yin, et al. 2002) (Miao, et al. 2005).

1.6.4. Hydrothermal Synthesis

1.6.4.1 Definition of Hydrothermal Synthesis

Hydrothermal synthesis has been one of the most important techniques for fabrication of different types of product. This trend still continues for fabrication of nanomaterials. Although it is a very popular technique, there is no certain definition of it. Briefly, it can be explained as; dissolving and recrystallizing materials that are relatively insoluble at normal conditions by high pressure and temperature in the presence of aqueous solvent or mineralizers.

From hydrothermal method has been discovered to today there are so many different definitions are in literature. According to Lobachey, it is a group of methods in which crystallization is carried out from superheated aqueous solutions at high pressures (Lobachey 1973). Another definition is, hydrothermal synthesis is heterogeneous reactions above 100^oC and 1 bar in aqueous media made by Rabenau (Rabenau 1985). Laudise defined as; the growth from aqueous solution at ambient conditions (Laudise 1970). In 1994, Roy approach a bit differently than the others as; hydrothermal synthesis is using water as catalyst and occasionaly as component of solid phases in the synthesis at greater than 100^oC and a few atmosphere (Roy 1994).

According to all definitions from past to nowadays, hydrothermal method can be described as heteregeneous reactions in the presence of water above room tempereature and 1 atm pressure in a closed system (Byrappa and Adschiri 2007)

1.6.4.2 History of Hydrothermal Synthesis

Especially for the last quarter hydrothermal synthesis has been used by different disciplines with an increasing interest. The first used of hydrothermal method was at 18th century by Scottish geologist Sir Roderick Murchison. Defining the changes on crusts of earth was his aim for using hydrothermal method (Sir Roderick Murchison 1840).

Various types of minerals are formed in water at elevated pressure and temperature conditions and this phenomenon is called as 'of hydrothermal origin'. Another example for 'of hydrothermal origin' is single crystals both formed in nature and made in laboratory. With the understanding of the mineral formation in nature under elevated pressure and temperature conditions in the presence of water, the hydrothermal technique has developed.

The first usage of hydrothermal method in chemistry was performed by Robert Wilhelm Bunsen in 1839. He synthesized barium carbonate crystals and strontium carbonate crystals in thick walled glass tubes at temperatures above 200^{o}C and at pressures above 100 bars (Bunsen 1848).

After World War II, the hydrothermal method became important for industrial growth of extremely pure crystals with interesting physical properties (Laudise and Ballman, 1969). Today there are several dozen companies throughout the world that produce α-quartz commercially more than 500000 kg each year (Jessop and Walter, 1999). Improvements in electronic industry required new materials, especially as a single crystal, and this necessity made hydrothermal method important.

1.6.4.3 Importance of Water in Solvothermal Synthesis

Although all the principles are same, the difference between solvothermal and hydrothermal methods is caused by water as solvent. Existing of water as solvent in hydrothermal method is provided many advantages.

First of all water is an environmental benefit as minimizng pollution and water can be volitilized easily and be recycled (Komarneri 2003) and compared to other solvent water is cheaper. When pressure and temperature are adjusted it can be catalyzed the precursor to desired materials (Byrappa, et al. 2001). Under hydrothermal

conditions, it is hard to dissolve some reactants in water and this handicap can be removed by supplementing mineralizers or solvents. Mineralizers quicken the reaction rate and crystal formation. They provide to raise ability of the compound solubility in water. The hydroxides of alkali metal salts like NaOH, KOH or LiOH, alkali salts of weak acids or elemental acids are used as mineralizers.

There are two critic parameters for solvothermal method and these are temperature and pressure, especially synthesizes occurs in a closed system with constant volume. So the pressure-temperature relations of solvents, for hydrothermal method it is water, should be known very well. In Figure 1.12, the critical point marks the end of liquid-vapor coexistence curve at the critical temperature, T_c, and pressure, P_c, in a phase diagram for a pure homogenous substance. If a fluid is reached the values above the its critical pressure and temperature, it is became a super critical fluid. The properties of supercritical fluids vary depending on the temperature and pressure, and it is an intermediate between a gas and a liquid. The increase in the temperature is made the liquid less dense and at the same time the gas become denser. When it reaches to the critical point the densities are equaled. Above the critical point, the compound becomes supercritical fluid and the phases of liquid and gas are not distinguishable.

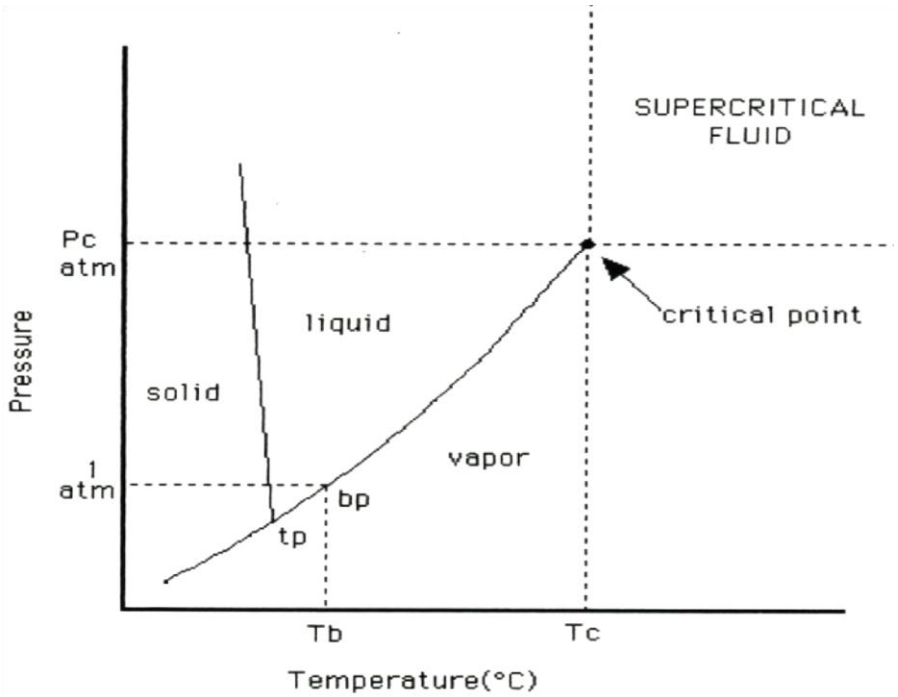

Figure 1.12. Phase diagram of water.
(Source: Şahin 2004)

The dielectric constant that is defined as the ability of a solvent to charge separate increases sharply with the pressure in the compressible region that refers to the area around the critical point in which compressibility is considerably greater than would be forecasted from the ideal gas law. This behavior is also parallel to a change in density, as shown in Figure 1.13. Density changes sharply but continuously with pressure in the compressible region. One of the most important advantages of hydrothermal solvents is that a change in density affects the solvating power. A decrease in the density results in a significant change in solvating ability.

Diffusivity and viscosity symbolizes transport properties that influence rates of mass transfer. These features are at least an order of magnitude higher and viscosity is lower compared with a liquid solvent. This means that diffusivity of species in SCF will occur faster than that obtained in a liquid solvent, which means that solids can dissolve and migrate more rapidly in SCFs. High diffusivity, low viscosity and intermediate density increases the rate of the reaction (Jessop and Walter 1999)(Eanes 2000).

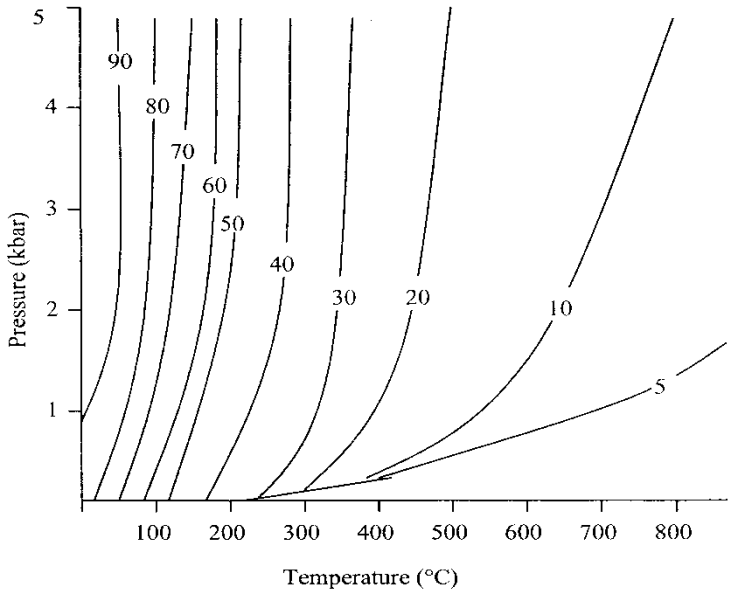

Figure 1.13. Variation of dielectric constant of water with pressure and temperature. (Source: Şahin 2004)

1.7. Surfactant

Surfactants are usually organic compounds that are amphiphilic, meaning they contain both hydrophobic groups (their tails) and hydrophilic groups (their heads)(The Lipid Chronicles 2012). The primary classication of surfactants as cationic, anionic, nonionic and zwitterionic (amphoteric) is made on the basis of the charge of the hydrophilic group, which is either ionic or nonionic (Jönsson 1998). The hydrophobic group is normally a hydrocarbon chain and the majority of these are linear to meet the demands for biodegradability.

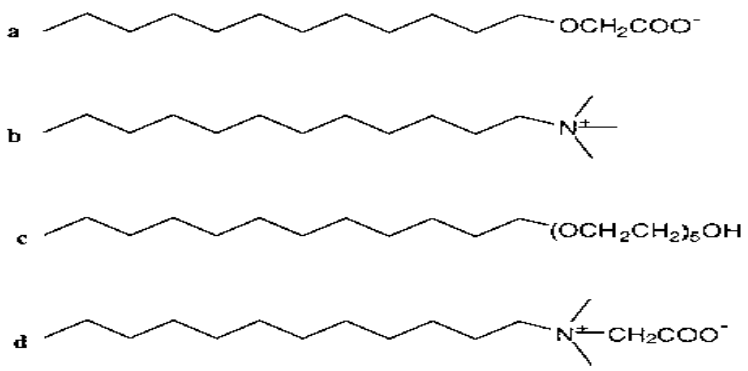

Figure 1.14. Structures of some representative surfactants: a) Anionic b) Cationic c) Non-ionic d) Zwitterionic

A surfactant is characterized by its tendency to adsorb at surfaces and interfaces. Examples of interfaces involving a liquid phase include suspension (solid-liquid), emulsion (liquid-liquid) and foam (liquid-vapour). In many formulated products several types of interfaces are present at the same time. Another general and fundamental property of surface active agents is that monomers in solutions tend to form aggregates, called micelles (Jönsson 1998). Micelles form already at very low surfactant concentrations in water. In Figure 1.15, behaviour of surfactant molecules at different concentration values are shown. The concentration at which micelles start to form is called critical micelle concentration (CMC). Micelle formation, or micellization, can be viewed as an alternative mechanism to adsorption at the interfaces for removing hydrophobic groups from contact with the water, thereby reducing the free energy of the system. It is an important phenomenon since surfactant molecules behave very differently depending on whether they are present in micelles or as free monomers.

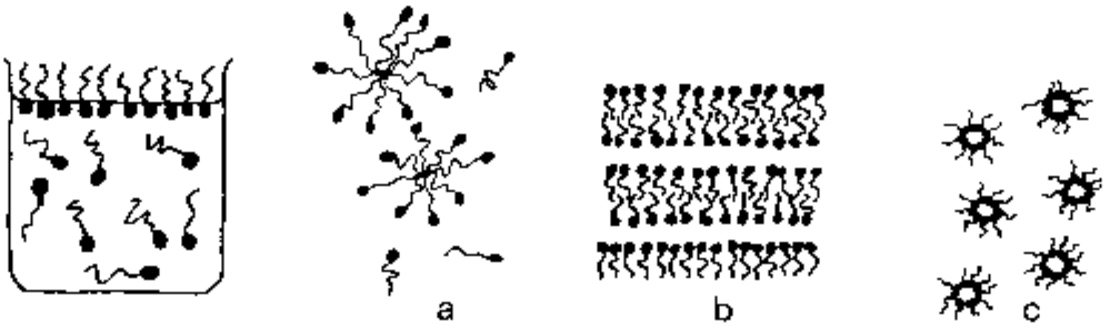

Figure 1.15. Illustration of surfactant molecules in a solution at low concentration. Above the CMC concentration (a) micelles is formed. At higher surfactant concentration, the amphiphiles form a variety of structures, here illustrated with (b) a liquid crystalline lamellar single-phase and (c) reversed micelles, an isotropic single-phase.

The micelles behave as large molecules and influence the solubility of organic hydrocarbons and oils in aqueous solution and also influence the viscosity. The size of the micelle is measured by the aggregation number which is the number of surfactant molecules associated with a micelle. Only surfactant monomers contribute to surface and interfacial tension lowering. Wetting and foaming are governed by the concentration of free monomers in solution.

1.8. The Purpose of the Study

In this study, the first aim is to synthesize cerium oxide (CeO_2) nanoparticles by hydrothermal method and observe the effect of base type, surfactant type, reaction temperature, reaction time and concentration on morphology and size of the particle.

For the second part, these synthesized nanoparticles will be used as catalyst for flavon synthesize from 2'hdroxychalcone. Catalytic properties of cerium oxide nanoparticles will be investigated.

CHAPTER 2

EXPERIMENTAL METHODS

2.1. Reaction Autoclaves

The basis of the hydrothermal method depends on high temperature and high pressure. To achieve these parameters a close system is needed. This system is autoclave. These autoclaves have some properties as;

1) Inertness to chemicals that are used.

2) Leak-proof to reach the desired temperature and pressure.

3) Long-time duration.

PTFE (polytetrafluoroethylene) lined acid digestion bombs were used in this study and these reaction autoclaves were provided from Parr Instrument Company (Illınois, USA) and removable Teflon was used as a lining material. Its volume was 23 ml and maximum reaction conditions were 240^{o} C and 1800 psi. The closure design consists of a spring-loaded, broad flanged closure that is sealed by tightening the bomb cap with a hook spanner wrench (Figure 2.1). Due to the larger coefficient of thermal expansion of Teflon (the liner) versus metal (the material in which the liner is enclosed), the Teflon will expand and contract much more upon heating and cooling cycles than its enclosure material. Therefore, a spring-loaded closure is used to maintain a constant pressure on the Teflon seal during both heating and cooling cycles.

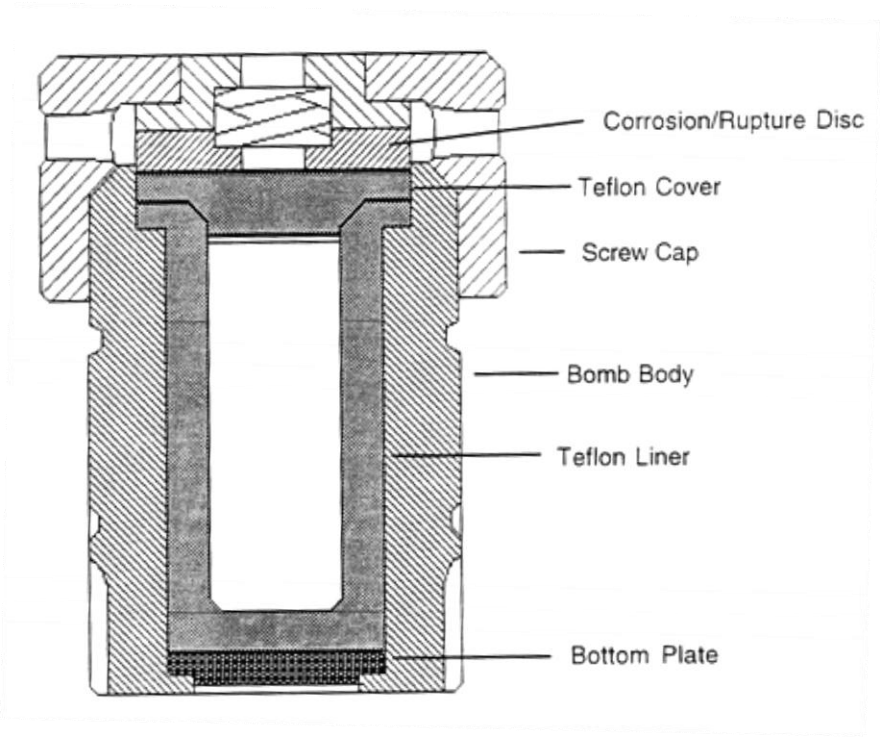

(a)

(b)

Figure 2.1. (a) Schematic representation of an autoclave, (b) Parr acid digestion bomb. (Inset shows the Teflon liner).

The temperature, solutions' nature and the degree of filling is changed the pressure inside the autoclaves in hydrothermal synthesis. Working on maximum temperatures is decreased the durability of autoclaves. Also, when filling the teflon line above the 80% of volume, because of solutions tend to expand, it is filled all volume

and there is no sufficent space for vapor. Figure 2.2 shows the behavior of water at different temperature.

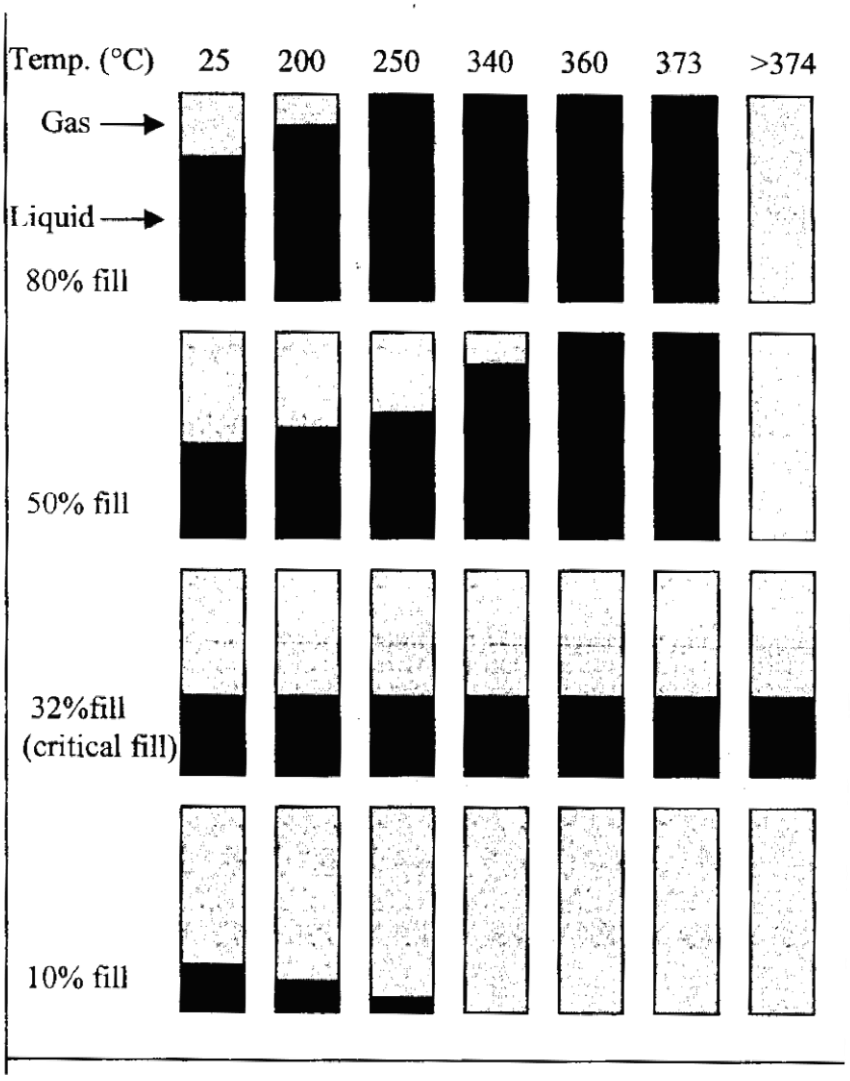

Figure 2.2. Pressure-Temperautre behavior of water at various degrees of fill. (Source: Laudise 1987)

2.2 Characterization Techniques

In this study, ceria is the main topic and it is a metal oxide which is a part of a inorganic field. For determining the characterization technique firstly it must known that material is moleular or non-molecular. For molecular type of substance, chemical analysis and spectroscopic methods are used to identification, yet it is non-molecular

and crystalline generally X-Ray diffraction and electron microscopy (SEM/EDX) are used to identification.

For crystalline structure substance X-Ray diffraction patterns are like fingerprints. Most of the inorganic solids X-Ray diffraction patterns are known and unknowns can usually be identified rapidly.

In this study, X-Ray diffraction, SEM and TEM are used to identificate the CeO_2 nanoparticles. TLC, GC-MS and MNR are used to identificate the organic substances.

No single technique is capable of providing a complete characterization of a solid. There are three main categories of physical technique that may be used to characterize solids; these are diffraction, microscopic and spectroscopic techniques. In addition, other techniques such as thermal analysis, physical property measurements may give good information.

2.2.1 X-ray Powder Diffraction

X-Ray diffraction (XRD) is one of the best methods to characterize solids and investigate its crystal structure. Also the orientation of both single crystals and defects in crystal structure are done by using X-Ray diffraction method (Cao 2004) . Powder, crystal and other forms of solids can be studied by X-Ray diffraction (Tanaka and Suib, 1999).

X-Ray region has unit of measurment which is the angstrom (A^o), equal to 10^{-8} cm, and X-Rays used in diffraction have wavelengths lying approximately in the range 0.5-2.5A^o (Cullity 1956). Under the high voltage system, high speed electron with a metal target collided to produce X-rays in X-ray tube. Beam of X-rays fall on a specimen as it generated, the crystalline phases in the specimen are diffracted. Figure 2.3 shows the typical X-Ray diffraction instrument.

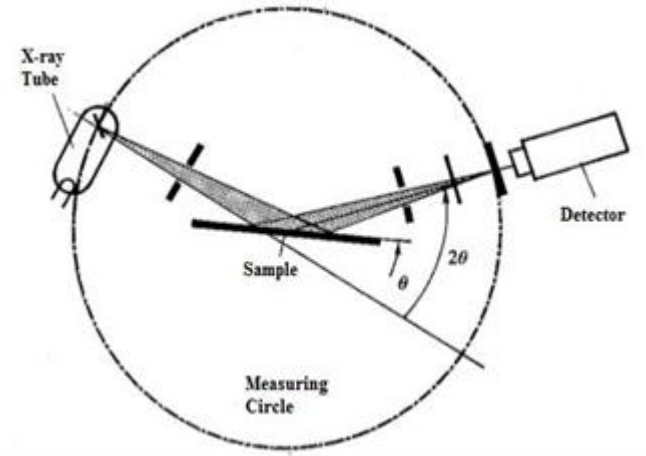

Figure 2.3. The X-Ray Spectrometer.
(Source: Smart and Moore)

The diffraction is occured according to the Bragg's law:

$$n\lambda = 2d \sin\theta \tag{2.1}$$

where n is the order of reflection, λ is the wavelegth of incident x-ray, d is the interplanar spacing between planes of a crystal and θ is the angle between incident beam and specimen surface (Cullity 1978).

Diffracted X-ray intensity is measured kind of function of the diffraction angle, 2θ and the specimen's orientation. This diffraction pattern is used to obtain information of the structural properties and to define the specimen's crystalline phases. It is a group of lines or peaks that has discrete intensity and position. These intensities are charactrestic feature of a material. Cerium oxide x-ray diffraction pattern can be seen in Figure 2.4.

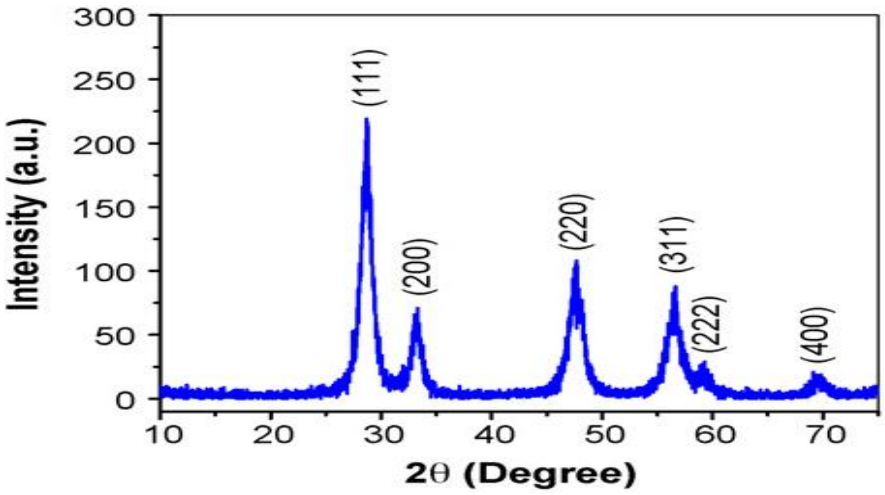

Figure 2.4. Typical XRD spectrum of cerium oxide nanoparticles.
(Source: Phoka 2009)

Acquired diffraction patterns are compared with the known published patterns and if it is a common type, it is paired one of those known patterns. Crystalline substances with standard patterns are expensed in the powder diffraction file, JCPDS (Joint Committee on Powder Diffraction Standards). This database includes more than 35000 entries and enhances every year. Whether powder diffraction pattern has never been aggregated before, some hypotheses can be made on structural type (Smart and Moore, 1996).

The diffraction pattern is also given information about average crystal size (D). The Debye Scherrer's formula is used for that and it is applied to the most intense peak:

$$D = \frac{0.9\lambda}{B\cos\theta_B} \tag{2.2}$$

where λ is the wavelength of radiation, B is the full width at half maximum (FWHM) of the Bragg peak on the 2θ scale in radians and θB is the Bragg angle.

In this study, X-ray powder diffraction (XRD) measurements were done by using Philips X-pert Pro Powder Diffractometer with CuKα radiation. (λ=1.5406 Å) Source of X-ray is the Philips high intensity ceramic sealed tube and data was collected for 2θ values of 20° to 80°.

2.2.2 Scanning Electron Microscopy (SEM)

Scanning electron microscopy is one of the electron microscopy that scanning the surface of solid with a focus beams of electrons to produce its image. The interaction between these electrons and atoms on the surface is produced signals that can be detected by detectors and is given the information about surface tophography and composition. Energy of the electron beam can be changed between 100 eV to 100000 eV. The electron beams are focused to a spot that sized 0.4nm to 5nm by one or more condenser lenses.

When the electron beams contact with the surface of the sample, backscattered, Auger and secondary electrons are produced. Both secondary electrons and backscattered electrons should be taken in to consideration to study the surface. (Strobel and Heineman 1989)(Skoog, et al. 1998). Secondary electrons emit the surface electrons on the other hand backscattered electrons are reflected source electrons. These emitted and reflected electrons are detected in photomultiplier tube and 2D or 3D image is illustrated on the monitor. The schematic of Scanning Electron Microscopy is illustrated in Figure 2.5.

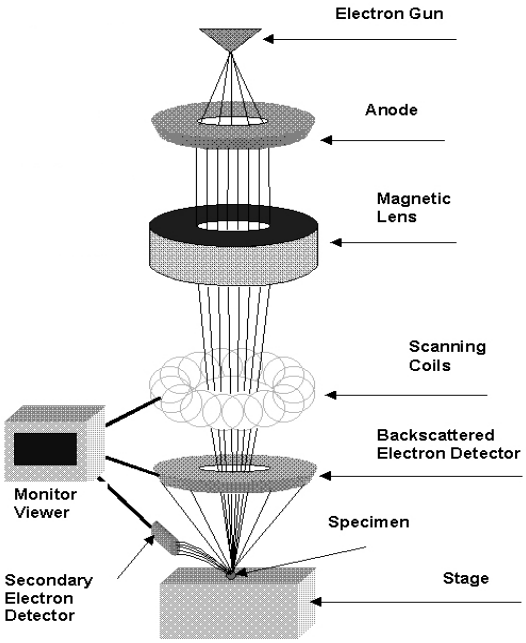

Figure 2.5. Schematic of Scanning Electron Microscopy.
(Source: Renssealer Polytechnic Institute 2007)

In this study Philips XL-30S FEG model instrument was used. The powder samples were attached on to carbon tapes supported on metallic disks. With the different magnifications, sample surfaces were scattered and the images were illustrated.

2.2.3 Transmission Electron Microscopy (TEM)

Transmission electron microscopy is a type of electron microscopy unlike scanning electron microscopy, image is formed by transmitted a beam of electron through a specimen. Electrons are emitted in the electron gun by thermionic or field emission. The latter are used when high gun brigthness and coherence are needed. A condenser lens system that includes three or four lenses is makes the sample illimunated. Some of the electrons are scattered and dissappeared from the beam due to the density of the material present in the sample. The electron-intensity distribution behind the sample (the unscattered electrons) is imaged by a three to eight stage lens system onto a fluorescent screen. The image can be recorded by direct exposure of a photographic emulsion or an image plate inside the vacuum, or digitally via a fluorescent screen coupled by a fiber-optic plate to a CCD camera. (Reimer, et al. 2008)

During transmission, the speed of electrons directly correlates to electron wavelength; the faster electrons move, the shorter wavelength and the greater the quality and detail of the image. The lighter areas of the image represent the places where a greater number of electrons were able to pass through the sample and the darker areas reflect the dense areas of the object. These differences provide information on the structure, texture, shape and size of the sample. The schematic of TEM is shown in Figure 2.6:

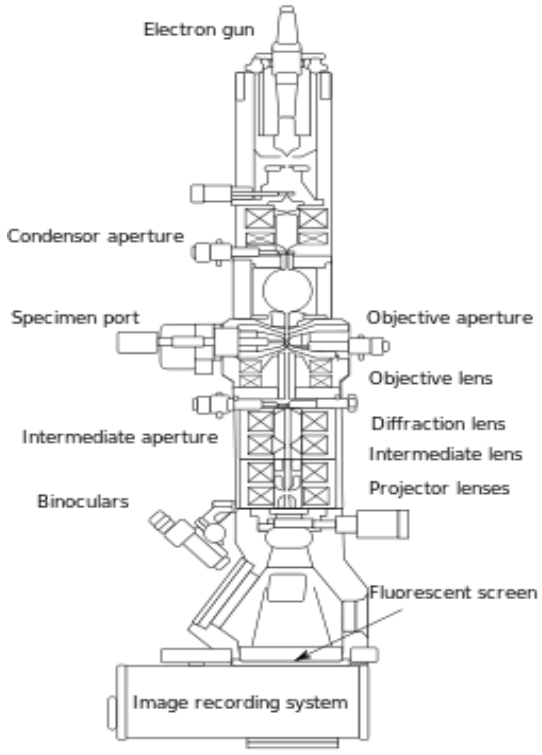

Figure 2.6. Shematic of TEM.
(Source: Wikipedia 2013)

2.2.4 Gas Chromotography-Mass Spectroscopy (GC-MS)

GC-MS is a combination of two instruments. Gas chromatography (GC) separates the components of a mixture, and mass spectrometry (MS) helps to identify these components. Basic design of the GC-MS instrument is shown in Figure 2.7.

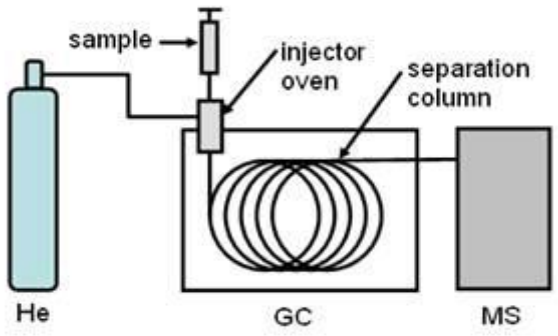

Figure 2.7. Basic design of GC-MS instrument.

Gas chromatography is a technique that used to identify mixture of compound by separating them according to their polarity. As with all chromatographic techniques, GC separations are based on compounds in a mixture being partitioned between two phases – one mobile and one stationary. The sample mixture is injected into an oven where it is vaporized. The mixture is then swept up by a stream of helium gas (the *mobile* phase) and carried to the coiled GC column. This column is a 30-meter long thin tube made of fused silica (SiO_2), the inner walls of which are coated with a film of liquid polymer (the *stationary* phase). As the mixture of compounds moves through the column, the individual components separate from each other as some compounds spend more time in the stationary phase and others more time in the mobile phase. This partitioning between phases is typically based on the relative polarity of the compound versus the polarity of the stationary phase. The more polar the compound, the more time it will spend in a polar stationary phase, and the less time it will spend in a non-polar stationary phase. Also, small compounds tend to move through the column faster than large compounds, just as it would be expected.

As the individual compounds emerge from the GC column, they are carried to the mass spectrometer. The mass spectrometer consists of three distinct regions: ionizer, mass analyzer, and detector. Compounds enter the ionizer and encounter a beam of electrons emitted from a filament. When the sample enters the ionizer, firstly the molecules are broken into fragments, and then these fragments are turned into ions by electrons bombard. The fragmented ions then encounter the quadrupole mass analyzer. The quadrupole consists of four parallel metal rods to which both a dc voltage and an oscillating radiofrequency voltage are applied simultaneously. This causes ions entering the poles to move in an oscillating path. If an ion has the correct mass-to-charge ratio (m/z), it will follow a stable (resonant) path between the rods. Ions without the correct m/z, however, will follow a non-resonant path and collide with the rods. By very quickly changing the values of the voltages applied to the rods, an entire mass range spanning several hundred mass units can be scanned in milliseconds. Resonant ions emerge from the quadrupole and hit the face of the detector where they eject electrons from the detector surface. These ejected electrons are carried through the detector, continuing to collide with the detector walls, creating even more ejected electrons and resulting in a measureable electrical current.

2.2.5 Nuclear Magnetic Resonance (NMR)

Nuclear magnatic resonance is a phenomenon that occurs when the nuclei of certain atoms are immersed in a static magnetic field and exposed to a second oscillating magnetic field. However the nucleus has a spin for that. It can be explained briefly as, subatomic particles (electrons, protons and neutrons) can be imagined as spinning on their axes. In many atoms (such as ^{12}C) these spins are paired against each other, such that the nucleus of the atom has no overall spin. However, in some atoms (such as ^{1}H and ^{13}C) the nucleus does possess an overall spin.

Mostly used NMR types are proton NMR (^{1}HNMR) and carbon NMR (^{13}CNMR). A proton NMR working principle is determining the energy change between two energy states of protons. The effect of magnatic resonance to the energy states of protons caused by the electrons around the protons, through the bonds and corresponding atoms. A compound can be identified by looking at the chemical shifts produced. Chemical shifts result from the "small magnetic fields that are generated by electrons as they circulate around nuclei" (Skoog, et al. 2008).

Carbon NMR is similar to that of proton NMR, but instead looks at the "magnetic environments of the carbon atoms themselves" (Wade 2009). Since the ^{13}C isotope is relatively rare, ^{13}C NMR is significantly less sensitive than ^{1}H NMR (Wade 2009). Although the carbon NMR has less sensitivity and that is made a disadvantage, it is become more important than proton NMR when concerning the backbone of a compound instead of the branches (Skoog, et al. 2008).

Varian 400-MR (400 MHz) was used to monitore the results of the reactions in this study.

2.3. Experimantal Procedure

2.3.1. Synthesis of Cerium Oxide Nanoparticles

In this study, two different approaches were followed to synthesize cerium oxide nanoparticles. These are with and without assiting of surfactants. Without assisting of surfactant, 0,5 g $Ce(NO_3)_3.6H_2O$ was dissolved in 15mL of distilled water and NaOH, and Urea solids' were added in it as required amount. For compare differnt

concentration of mineralizers, different amounts were used. The mixture was stirred about 20 minutes until it reached a homogeneous form and it transferred in to 23 mL teflon autoclave. Filling level of vessel was 70%. Hydrothermal method was applied all the samples at differnt temperatures and times. After the hydrothermal method was applied, the solution in the autoclave was transffered in to a 50mL falcon tube and washed with distilled water 3 times in centrifuge at 6000 rpm. Collected ceria nanoparticles were dried in oven at 70 ^{o}C for 24 hours.

By assisting of surfactant, similiar way was applied to synthesize ceriom oxide nanoparticles. 1,16 g of $Ce(NO_3)_3.6H_2O$ was dissolved in 15mL distilled water. Different types of polyethylene glycol (PEG2000, PEG4000, PEG6000 and PEG10000) were added as 0,03 mmol and different amount of mineralizers (Urea and NaOH) were added in to mixture finally. The mixture was stirred 20 min and transffered into 23 mL autoclave. Filling level of vessel was 70%. Hydrothermal method was applied at different temperatures and times. The solution in the autoclave was transferred to 50 mL falcon tube and washed 3 times with distiled water and ethanol in centrifuge. Collected nanoparticles were dried at 70 ^{o}C for 24 hours then calcined at 500 ^{o}C for 4 hours.

2.3.2. Activation of Cerium Oxide Nanoparticles

Synthesized ceria nanoparticles were activated to use in transformation of flavone from 2'-hydroxychalcone. To activate the ceria nanoparticles, they were treated with 8M NaOH solution in ultrasonic water bath and dried for 2 days in oven at 60^{o}C. Particles that were synthesized in the presence of NaOH were used in activation process because their size was ranged in nanoscale yet synthesized with urea had sub-micron range.

2.3.3. General Methods for Catalytic Transformations of Chalcones

2'-hydroxychalcone was commercial grade and used as supplied. Reactions were monitored by thin layer chromatography by using Merck TLC plates (Silica gel 60 F254). Chromatographic separations and isolations of compounds were performed by column chromatography. 70-230 mesh silica gel was used for column chromatography. Solvents were also commercial grade and were used as supplied. The

synthesized products were analyzed by GC-MS (HP 5MS, 25 m, 0.25 mm ID, inlet temperature: 290 ^{o}C, temperature programming: 40 ^{o}C, 5 ^{o}C/min, 300 ^{o}C (5min.), flow rate: 1.5 mL/min) and ^{1}H NMR data was recorded on Varian 400-MR (400 MHz) spectrometer. Chemical shifts for ^{1}H NMR is reported in δ (ppm). $CDCl_3$ peaks were used as reference in ^{1}H NMR (7.26 ppm).

2.3.4. Synthesis of Flavone

For the synthesize of flavone 2'-hydroxychalcone used as starting reagent, CeO_2 nanoparticles that treated with 8M NaOH solution used as both base and catalyst. The mixture of 30 mg 2'-hydroxychalcone **(1)** and 30 mg activated CeO_2 nanoparticles in anhydrous DMSO or DMF was prepared then stirred for 24 hours at 100 ^{o}C in reflux set-up. The resulting mixture was extracted with distilled water and ethyl acetate (3 x 20 ml). After seperating organic part, $MgSO_4$ was added to dried the solution and it was filtered. The solvent was evoporated by rotary evaporator and high pressure vacuum pump.

The crude product was purified by column chromotography on silica gel (1:15 EtOAc/Hexane solvent system) to isolate the flavone **(3)**. Rf = 0.25 (1:4 EtOAc/Hexane) or was analyzed by GC-MS.

CHAPTER 3

RESULTS AND DISCUSSION

3.1. Morphological and Structural Characterization

X-Ray Diffraction was used to determine the structure of synthesized particles. Unique XRD pattern of cerium oxide nanoparticles is shown in Figure 3.1. NaOH and Urea were used in order to synthesize nanoparticles. XRD pattern shows the characrteristics of CeO_2 and all the reflections are indexed to cubic fluorite structure (JCPDS – 81-0792) with a lattice parameter of 5.412 Å. Both Ce^{4+} and Ce^{3+} valance cations exist in bulk structure and as cerium oxide is reduced from 4+ to 3+ lattice constant increase, electrostatic forces between particles decrease the Ce^{3+} defect states can be observed from XRD pattern (Tsunekawa, et al. 2000). Therefore based on this information (and the Figure 3.1) CeO_2 nanoparticles synthesized with urea does not have considerable Ce^{3+} defects.

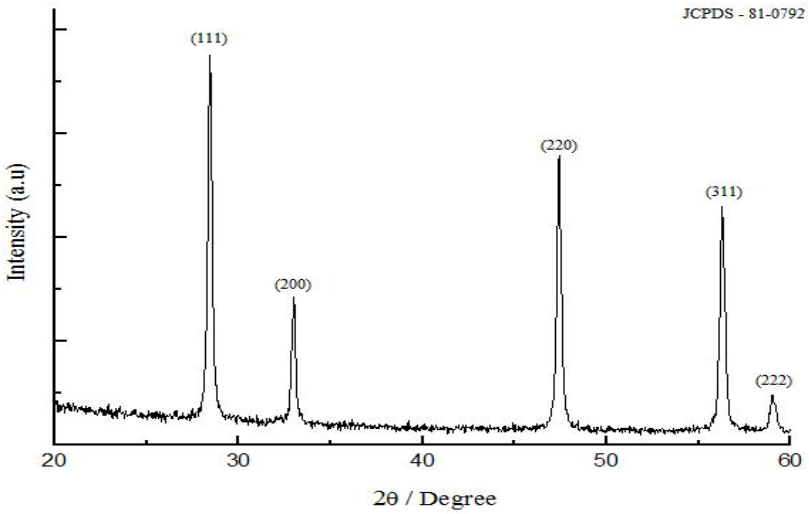

Figure 3.1. XRD pattern of as-prepared CeO_2 nanoparticles.

Generally partical morphology spherical, cubic and rod-like shape was observered by scanning electron microscopy. In Figure 3.2, SEM images of cerium oxide nanoparticles having different shapes are shown.

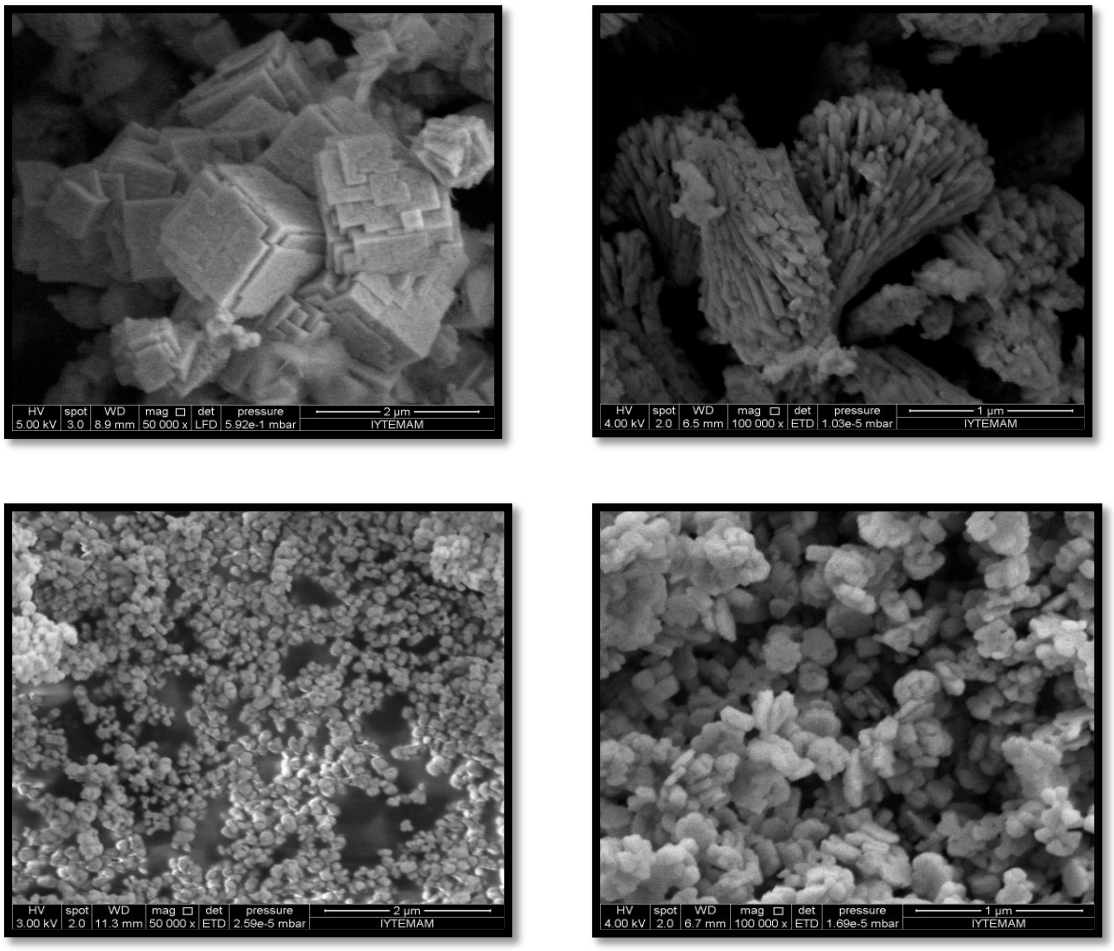

Figure 3.2. SEM images of Cerium oxide nanoparticles.

In Figure 3.3, TEM images on the fringe distance of cerium oxide nanoparticles synthesized by urea were shown. Based on the grain boundaries, agglomeration of the particles can be clearly seen in these images.

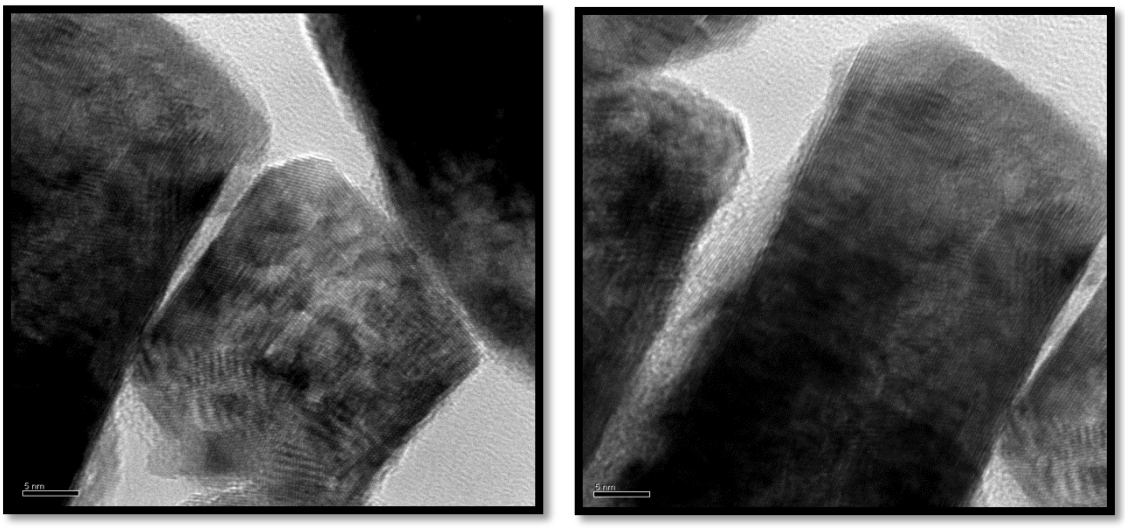

Figure 3.3. HRTEM image of single CeO_2 nanoparticles in the presence of 1M Urea for 8h at 180^{o}C.

3.2. Controlling Factors on Size and Shape of CeO2 Nanoparticles

In this study, effect of base type, concentration, surfactant, reaction time and temperature on size and the shape of nanoparticles was investigated.

3.2.1. Effects of Base Type, Surfactant and Concentration

During the study, NaOH was used for a strong base and urea was used for a weak base to see the effect of base type. The results obtained from study of particle and average crystal sizes were measured using SEM images and by using Debye-Scherrer equation respectively. Sizes of 100 particles (randomly picked) were measured by using ImageJ software to calculate the particle size. Particle size distribution graphs were drawn by using these data. The strongest peak of ceria (111) in XRD pattern was used to apply Debye-Scherrer equation. The equation is;

$$D = \frac{0.9\lambda}{B\cos\theta_B} \tag{3.1}$$

where λ is the wavelength of radiation, B is the full width at half maximum (FWHM) of

the Bragg peak (most intense peak) on the 2θ scale in radians and θ_B is the Bragg angle.

Based on SEM images, particles obtained using NaOH were smaller than particles obtained using urea. However crystal size of the particles synthesized using urea was smaller. One reason for the bigger particle size for urea particles were the agglomeration caused during calcination. In Figure 3.4, SEM images of CeO_2 particles synthesized using urea and NaOH were shown. XRD patterns (Figure 3.5) and particle size distributions (Figure 3.6, 3.7) for same samples were also shown.

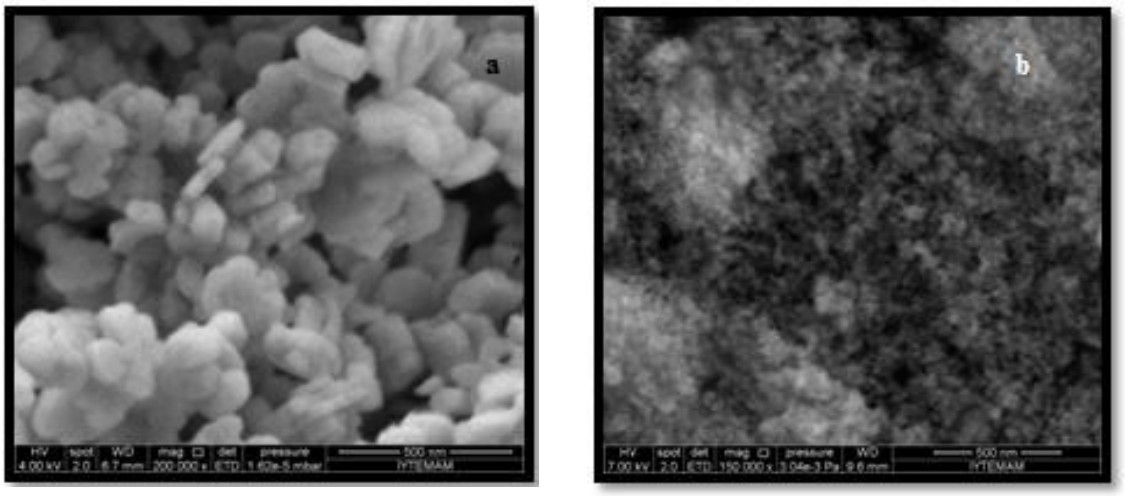

Figure 3.4. SEM images of (a) Urea (b) NaOH used CeO_2 nanoparticles at 180 ^oC for 8h.

In addition to size differences, the morphology of particles was very different from each other as well. While sphere-like particles were observed for NaOH, plates that in sub-micron range were observed for Urea. In Table 3.1, average crystal size and average particle size of NaOH and Urea used particles were given.

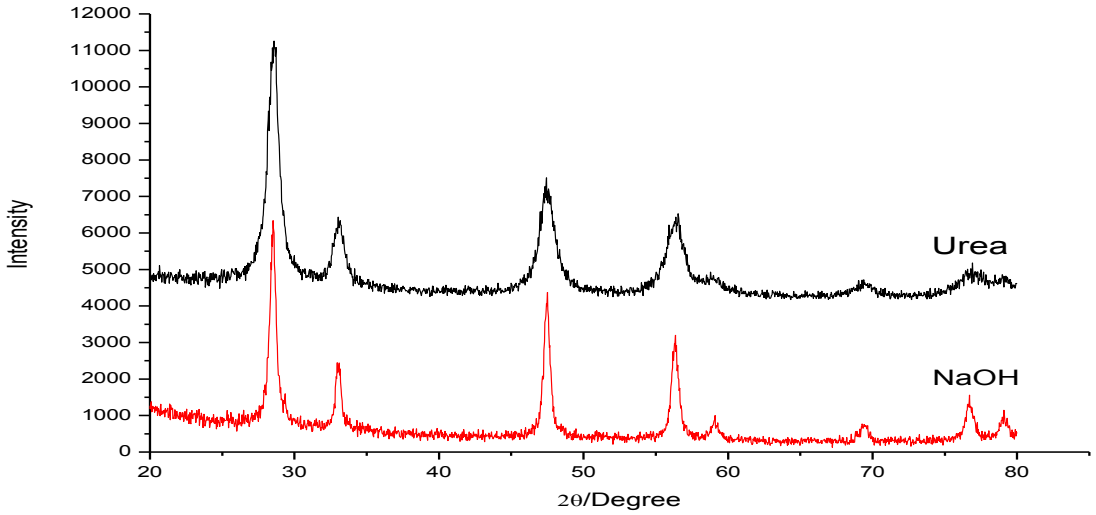

Figure 3.5. XRD patterns of as-prepared CeO_2 nanoparticles by Urea and NaOH at 180^{o}C for 8h.

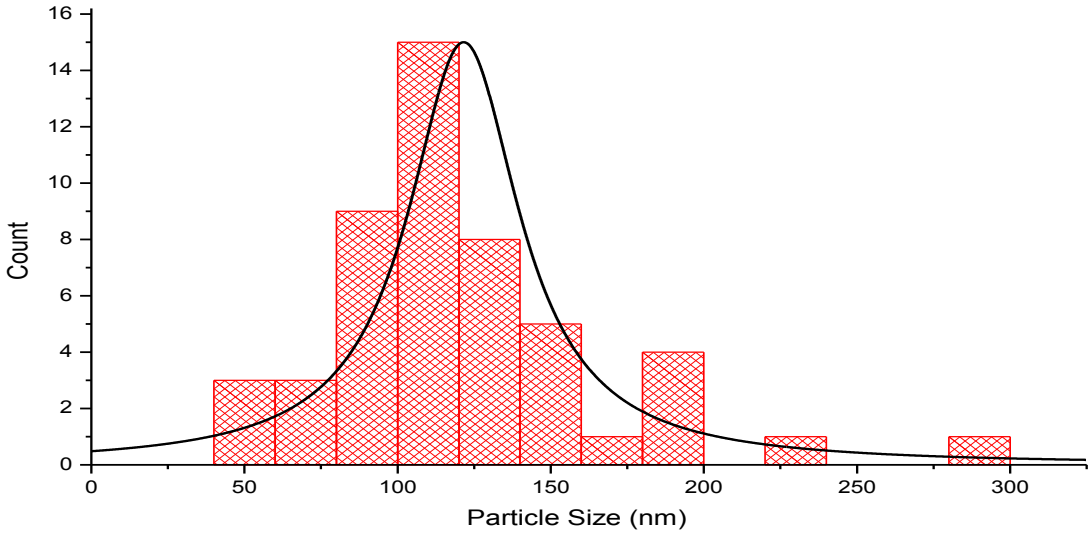

Figure 3.6. Particle size distribution of CeO_2 nanoparticles in presence of Urea.

Particles that were synthesized by Urea had size range between 50 nm and 200 nm generally. Also there were some particles 250 nm sized and 300 nm sized.

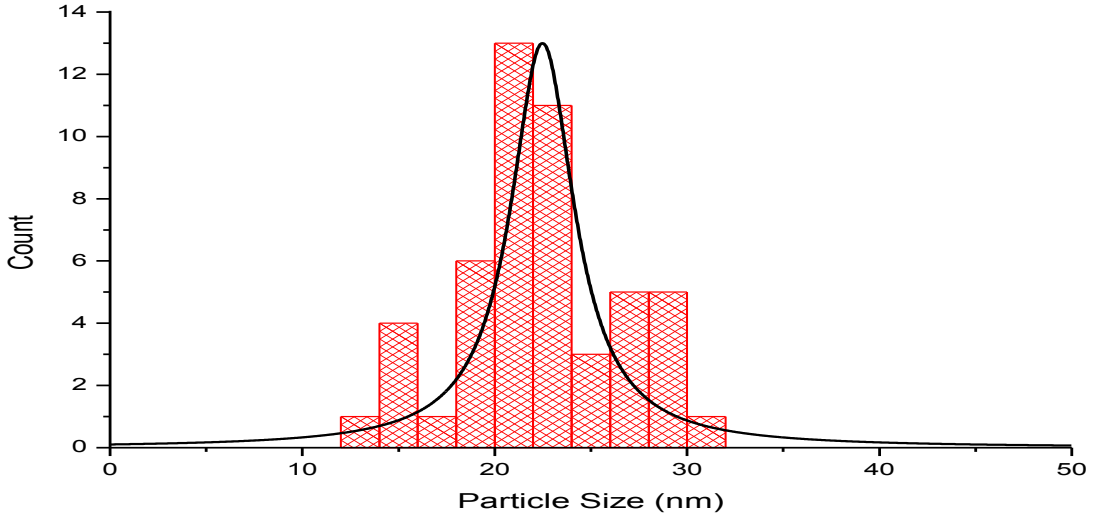

Figure 3.7. Particle size distribution of CeO_2 nanoparticles in presence of NaOH.

Particles that were synthesized by NaOH had size range between 13 nm and 30 nm.

Table 3.1. Average Crystal Size and Avearge Particle Size of CeO_2 nanoparticles were synthesized by Urea and NaOH at 180 ^oC for 8h.

Starting Base	Urea	NaOH
Average Crystal Size	11 nm	20 nm
Average Particle Size	125 nm	22 nm

The diference between crystal size and particle size for urea and NaOH can be explained the CeO_2 particles were formed in the presence of NaOH directly. However in the presence of urea under hydrothermal conditions, cerium carbonate particles were formed if the solution is neutral or basic. The formation of $CeOHCO_3$ precursor was given in the following reaction process (Hirano and Kato, 1999):

$$H_2N–CO–NH_2 \Leftrightarrow NH_4^+ + OCN^- \quad (3.2)$$

$$OCN^- + 2H_2O \rightarrow NH_4^+ + CO_3^{2-} \quad (3.3)$$

$$Ce^{3+} + yH_2O \rightarrow [Ce(OH)(H2O)_{n-1}]_2+ + H_3O^+ \quad (3.4)$$

$$[Ce(OH)(H_2O)_{n-1}]^{2+} + CO_3^{2-} = CeOHCO_3 + (n-1)H_2O \quad (3.5)$$

In this study, solution pH was 6,3 before hydrothermal treatment and after dissociation of urea the solution medium becames basic (Hirano and Kato, 1999) and after hydrotermal treatment cerium carbonate particles were obtained. Calcination was applied to cerium carbonate particles to form CeO_2 particles. To decrease the surface energies, particles were aggregated and grew into larger particles.

The effect of surfactant to the nanoparticles was invastigated and it can be said that there is no specific effect of surfactant to the particles crystal size that synthesized by Urea under hydrothermal conditions. On the other hand for NaOH used samples, the average crystal size became smaller. The effect of surfactant on particle size was also observed. Smaller particles were obtained in the presence of urea by using Surfactant yet in the presence of NaOH bigger particles were obtained by using surfactant probably because of calcination. In Table 3.2, the effect of surfactant to the crystal size and in Table 3.3 the effect of surfactant to the particle size is shown.

SEM images of CeO_2 nanoparticles synthesized with different surfactants were shown in Figure 3.8 and Figure 3.9. Particle size distribution of particles in the presence of Urea (Figure 3.10) and NaOH (Figure 3.11) with different surfactants was shown, as well.

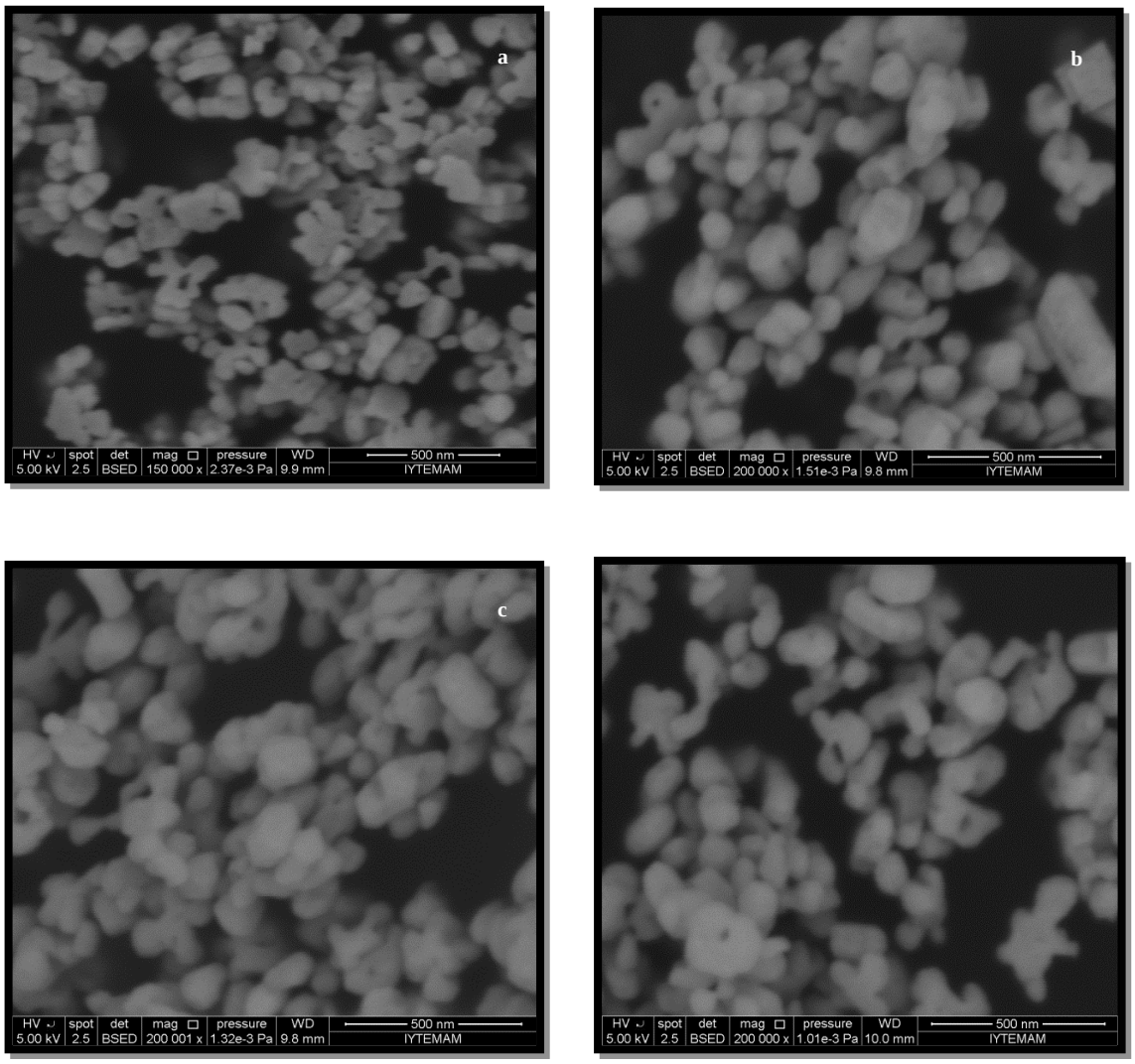

Figure 3.8. SEM images of CeO_2 nanoparticles synthesized with (a) PEG 2000 (b) PEG 4000 (c) PEG 6000 and (d) PEG 10000 by Urea at 180^{o}C for 8h.

Effect of surfactant on the particle size can be discussed as following. Firstly, PEG possesses the structure of a long ethoxy chain, and it may arise in the steric effect and prevent the particles from aggregation when PEG was absorbed on the surface of $CeOHCO_3$ particles. Secondly PEG on the crystal facets of $CeOHCO_3$ changes the relative surface free energies of the facets and may block sites essential to the incorporation of new growth units into the crystal lattice. Consequently, these two effects may change the crystal growth kinetics and then influence on the size of the particles (Li, et al. 2010). For NaOH used particles, that could be explained the smaller

crystal sizes yet to remove the surfactant calcination was applied to the particles and because of the aggregated particles bigger particle sizes were obtained.

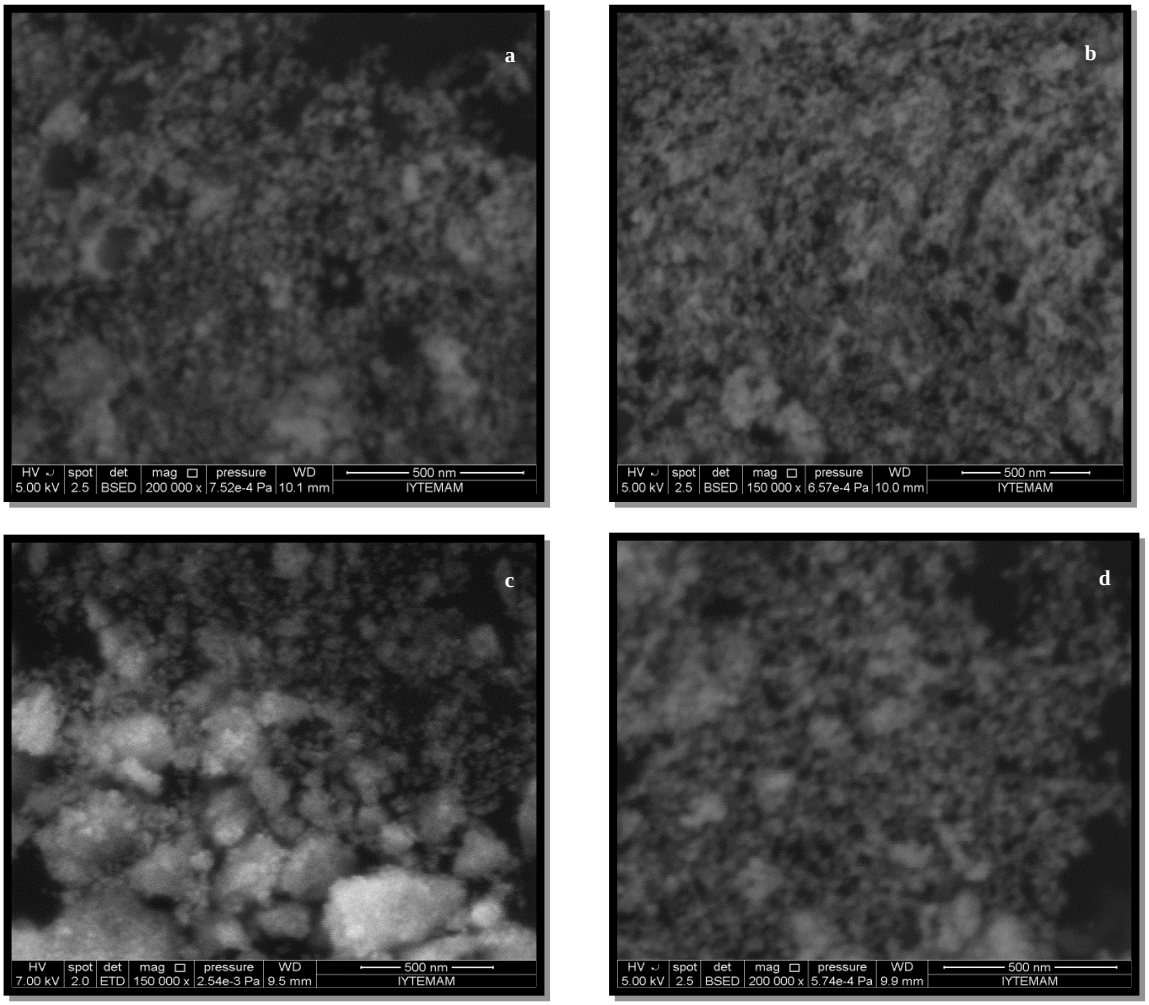

Figure 3.9. SEM images of CeO_2 nanoparticles synthesized with (a) PEG 2000 (b) PEG 4000 (c) PEG 6000 and (d) PEG 10000 by NaOH at 180^{o}C for 8h.

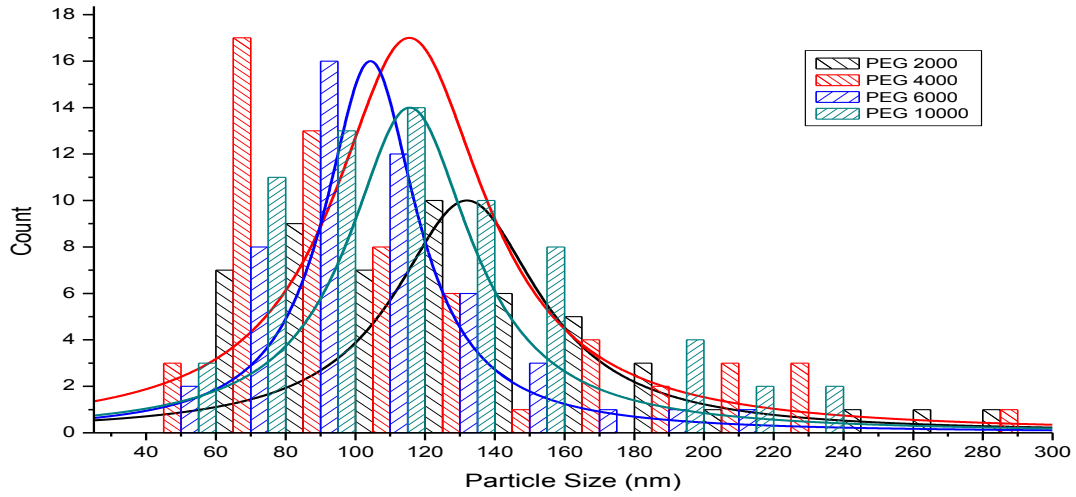

Figure 3.10. Particle Size distribution of CeO_2 nanoparticles in the presence of Urea with different surfactants.

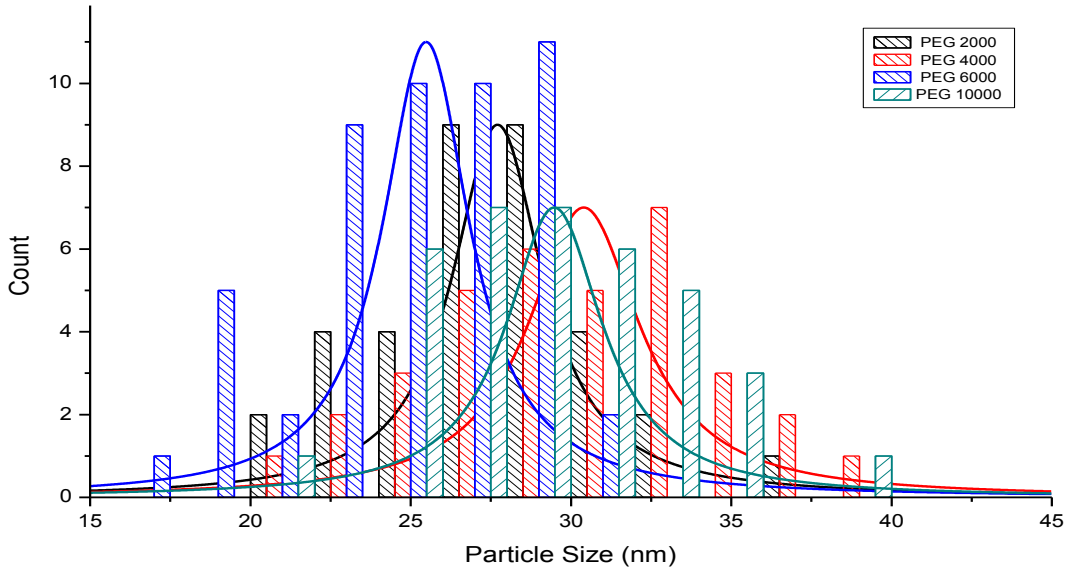

Figure 3.11. Particle Size distribution of CeO_2 nanoparticles in the presence of NaOH with different surfactants.

Table 3.2. Effect of surfactant to the average crystal size of CeO_2 nanoparticles.

Temperature: 180 °C / 8h. 1 M	Starting Bases	
Surfactants Type	Urea(nm)	NaOH(nm)
Without Surfactant	11	20
PEG (Mw:2000)	11	15
PEG (Mw:4000)	13	18
PEG (Mw:6000)	11	12
PEG (Mw:10000)	12	16

Table 3.3. Effect of surfactant to the average particle size of CeO_2 nanoparticles.

Temperature: 180 °C / 8h. 1 M	Starting Bases	
Surfactants Type	Urea(nm)	NaOH(nm)
Without Surfactant	125	22
PEG (Mw:2000)	130	28
PEG (Mw:4000)	120	30
PEG (Mw:6000)	105	25
PEG (Mw:10000)	115	29

The effect of surfactant on the morphology was not observed for particles synthesized with NaOH. Like in the particles synthesized without surfactant, spherical agglomerated particles were observed. For particles synthesized with urea, non-uniform cubic, spherical and plate shape particles were observed depending on the urea concentration.

The effect of concentration was investigated for particles that were synthesized by urea. There was an optimal value of concentration about1 M, lower than 1 M, both the crystal size and particle size became bigger and higher concentration than 1 M there were no specific change on the crystal size or particle size. Lower concentrations (0.1 M and 0.5 M) gave particles with defined morphology like cubes and triangular prism respectively. Figure 3.12 shows the SEM images of ceria nanoparticles that were synthesized at diferernt urea concentrations.

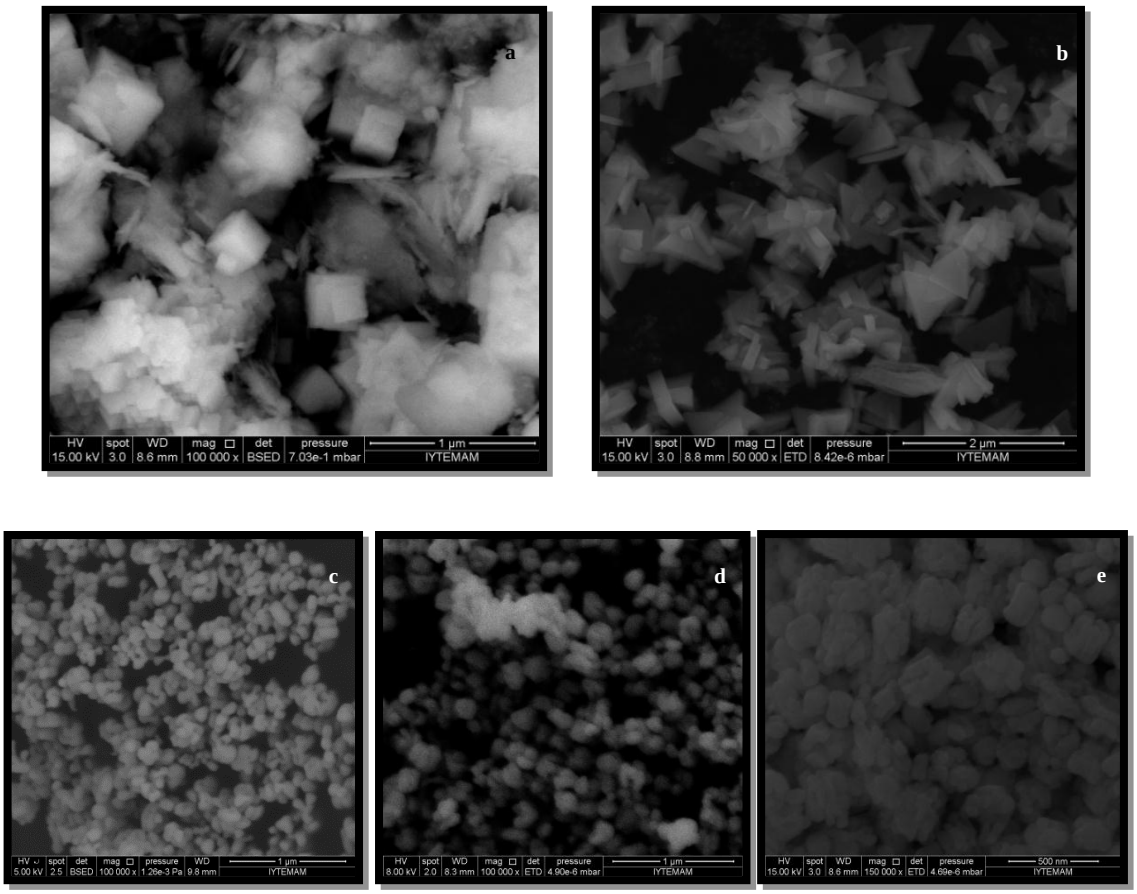

Figure 3.12. SEM images of CeO_2 nanoparticles that were synthesized at different urea concentration (a) 0.1 M (b) 0.5 M (c) 1 M (d) 1.5 M and (e) 3 M at 180^oC for 8h.

XRD patterns of ceriumoxide nanoparticles synthesized by urea at different concentrations were shown in Figure 3.13. In Figure 3.14, the particle size distribution of CeO_2 nanoparticles in the presence of urea at differerent concentrations and in Table 3.4, average crystal size, average particle size and morphology of CeO_2 nanoparticles synthesized by urea at different concentrations were shown.

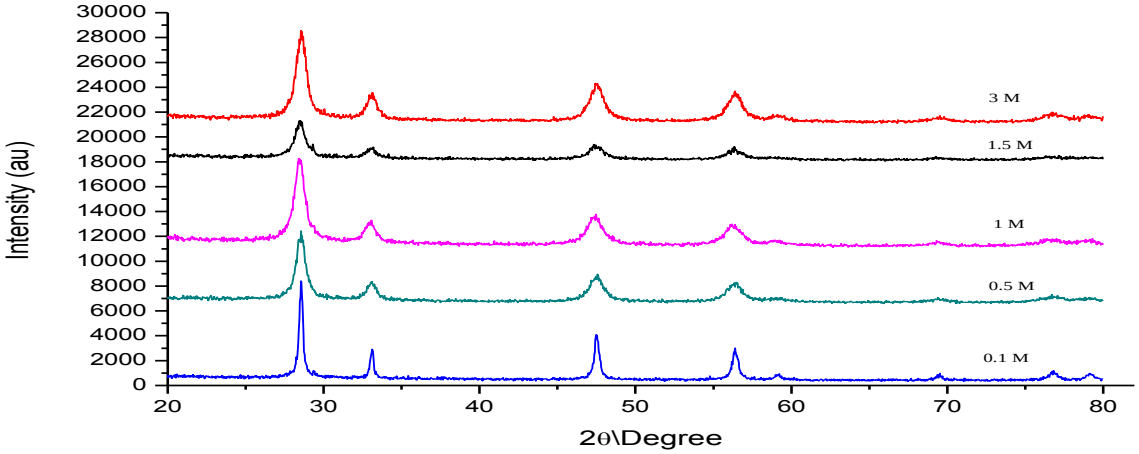

Figure 3.13. XRD Patterns of cerium oxide nanoparticles synthesized by different concentrations of Urea at 180°C for 8h.

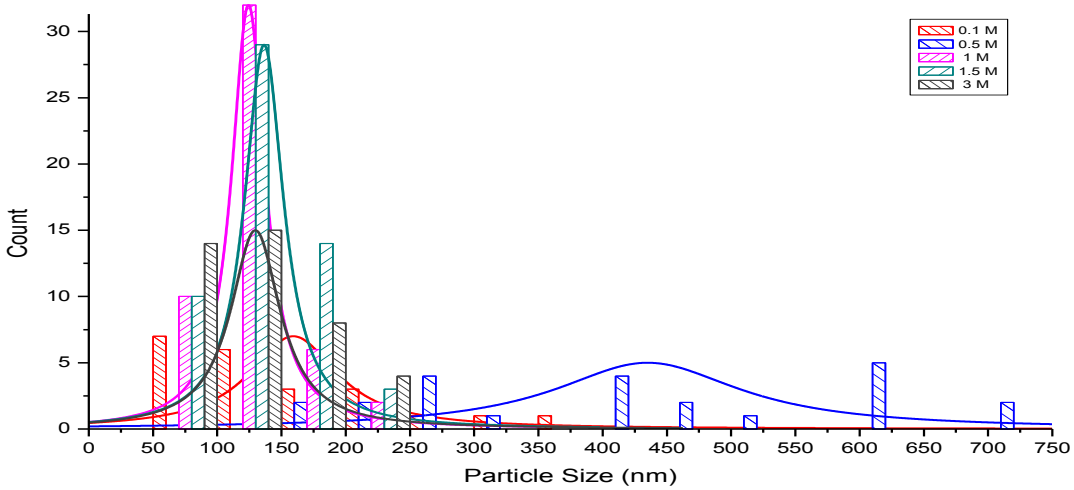

Figure 3.14. Particle size distribution of CeO_2 nanoparticles in the presence of Urea at different concentrations.

Table 3.4. Average Crystal Size, Average Particle Size and Morphology of CeO_2 nanoparticles synthesized by Urea at different concentrations.

Temperature 180 °C / 8h. 1M			
Concentration (M)	Avg. Crystal Size(nm)	Avg. Particle Size(nm)	Morphology
0,1	32	160	Cubic
0,5	14	440	Triangular prism
1	11	125	Spherical
1,5	12	133	Spherical
3	12	130	Spherical

The change on the concentration of urea was also changed the pH of the solution. It is likely that the increase in crystallite size is due to a decrease in the nucleation in the acidic solution as the solution becomes acidic by a decrease in the urea concentration (Hirano and Kato, 1999).

3.2.2. Effect of Reaction Time & Temperature

In this part of the study, reaction times and temperatures have been changed in order to understand the formation process of cerium oxide nanoparticles. Cerium oxide nanoparticles were synthesized by urea for the time interval of 1h, 12h and 24h.

Temperature-dependent experiments were also done at 60°C, 90°C, 120°C, 180°C and 240°C. In Figure 3.15, SEM images of CeO_2 nanoparticles synthesized by urea at different temperatures were shown.

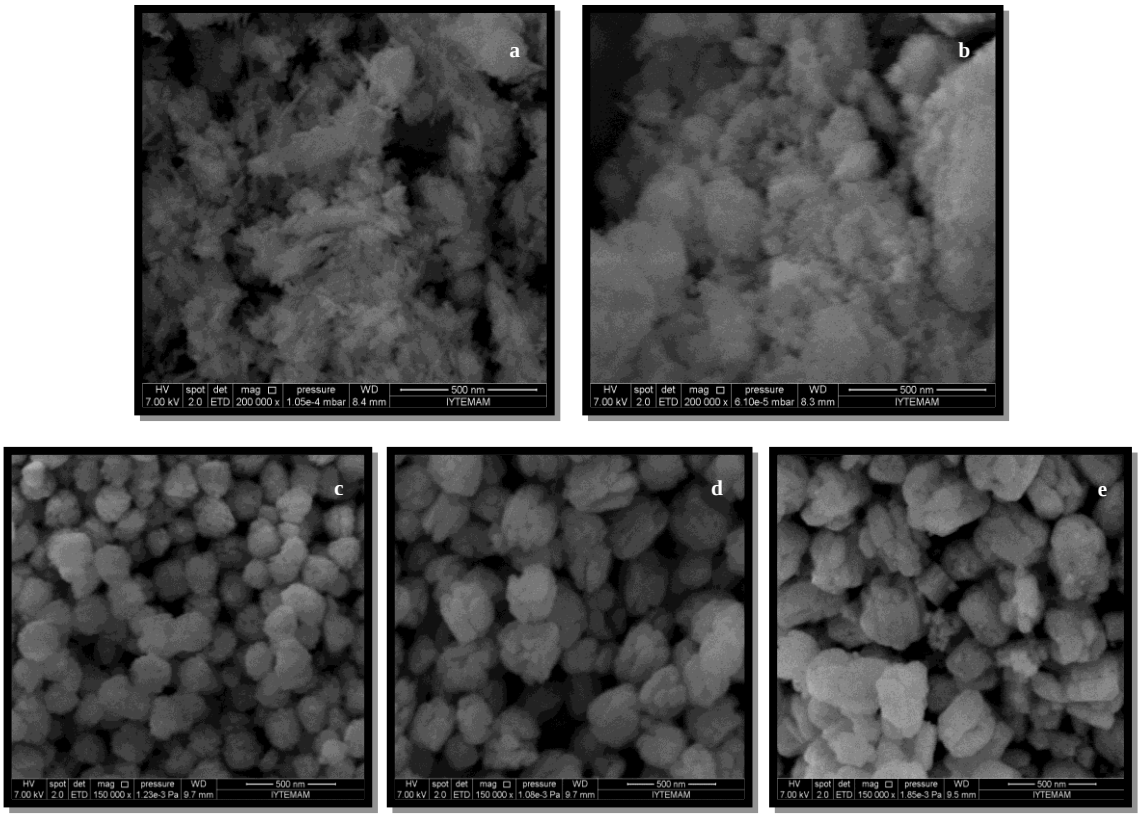

Figure 3.15. SEM images of CeO_2 nanoparticles synthesized by Urea for 24h at (a) 60°C (b) 90°C (c) 120°C (d) 180°C (e) 240°C

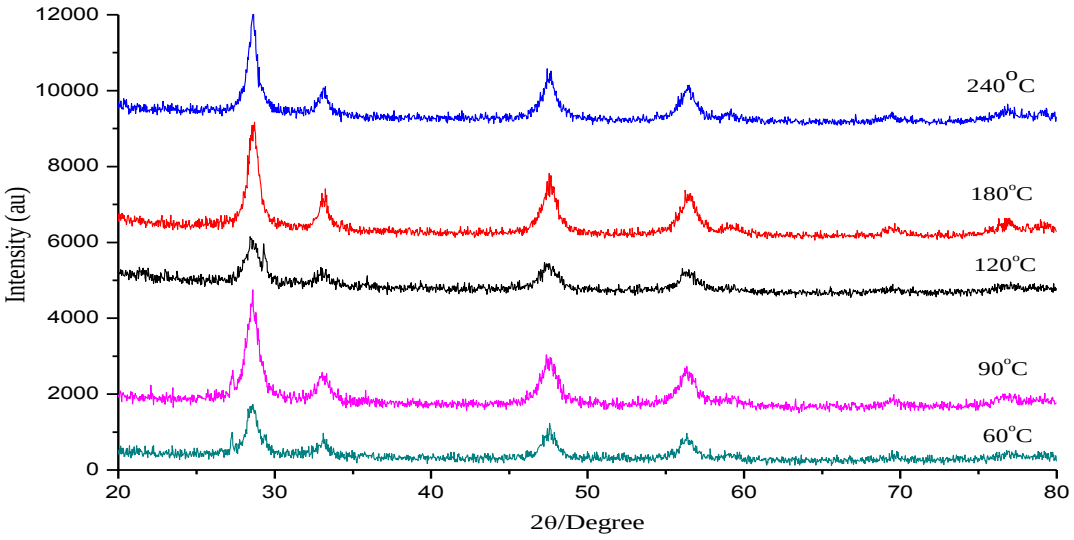

Figure 3.16. XRD Patterns of cerium oxide nanoparticles synthesized by 8M Urea for 24h at different temperatures.

While Figure 3.16 shows the XRD patterns of cerium oxide nanoparticles synthesized at different temperatures, particle size distribution graph that was drawn by using SEM images was shown in Figure 3.17.

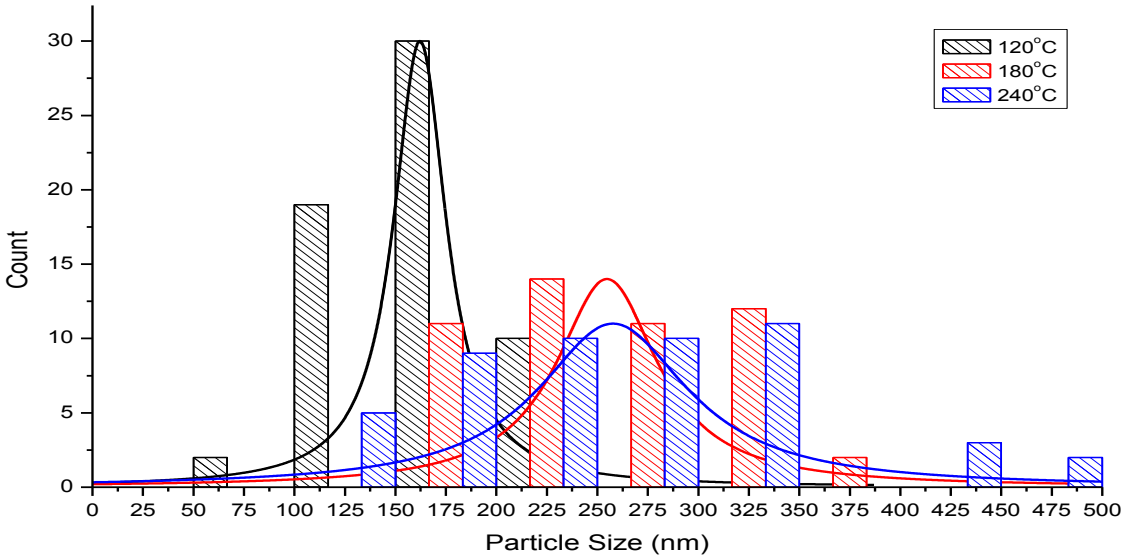

Figure 3.17. Particle size distribution of CeO_2 nanoparticles in the presence of Urea for 24h at different temperatures.

For particles that were synthesized at 60°C and 90°C, heavy agglomeration was observed and to give any particle size was not possible. However, according to their XRD patterns their average crystal sizes were about 10 nm.

Table 3.5. Effect of temperature on the crystal size.

Temperature(°C)	Avg. Crystal Size (nm)	Avg. Particle Size (nm)
120	6,5	165
180	12	260
240	14	260

As it can be seen in Table 3.5, the increase at temperature was caused both increase in nucleation and agglomeration so the crystal size and particle size were increased proportional to increase at temperature.

Reactions were performed for 1h, 12h and 24h to determine the effect of reaction time. Figure 3.18 shows SEM images of CeO_2 nanoparticles obtained at 240 ^oC with different reaction time. After reacting for 1h, the sphere-like morphology was obtained, which was assembled by rectangular prism shape particles with non-uniform size. Assembled non-uniform sphere-like morphology was obtained when reaction time was 12h and the decrease in the particle size was observed clearly. Similiar particle morphology was observed for 24h reactions, like in 12h reactions.

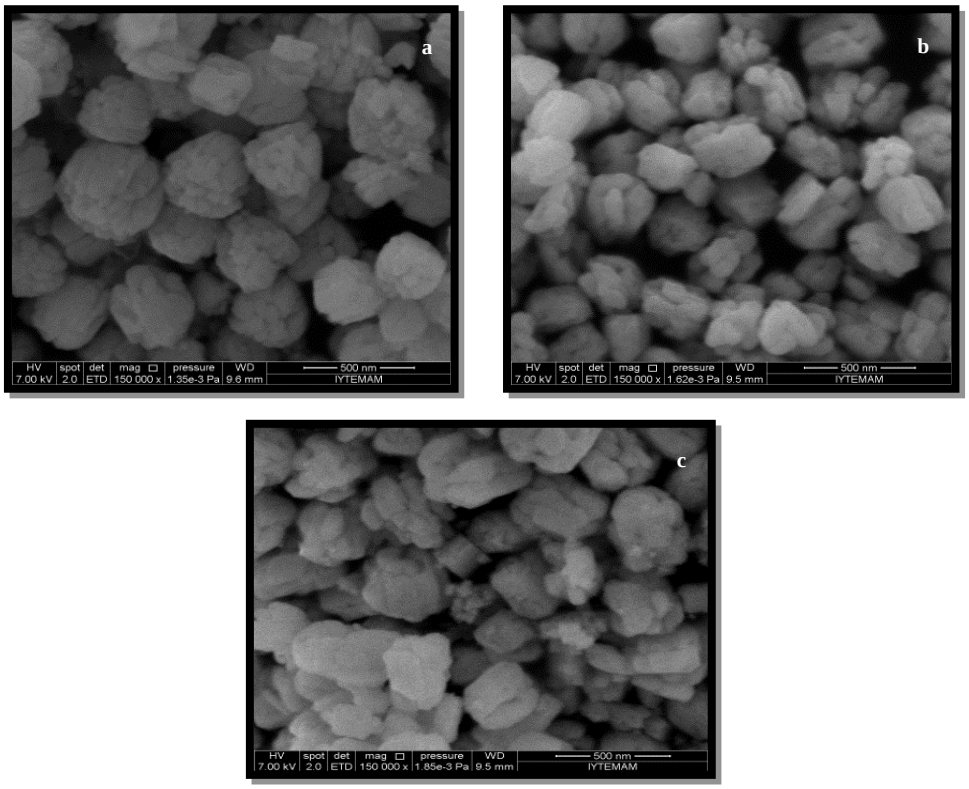

Figure 3.18. SEM images of CeO_2 particles that were synthesized by Urea at 240^o C for (a) 1h (b) 12h (c) 24h.

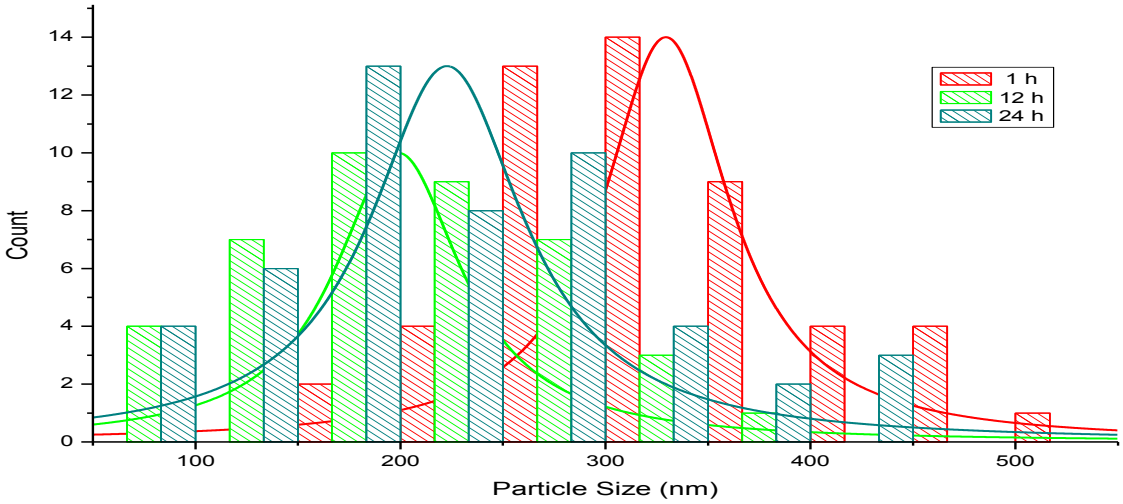

Figure 3.19. Particle size distribution of CeO_2 nanoparticles in the presence of Urea at 240°C for different reaction times.

Table 3.6. Average Crystal Size and Average Particle Size of CeO_2 nanoparticles were synthesized for different times.

Time (h)	Average Crystal Size (nm)	AverageParticle Size (nm)
1	15	335
12	13	200
24	14	225

Particle size distribution of CeO_2 nanoparticles for different reaction times is shown in Figure 3.19. and in Table 3.6., average crystal size and particle size of CeO_2 nanoparticles for different reaction times was shown.

3.3. Catalytic Property of CeO_2 Nanoparticles

In this study, the catalytic properties of ceria nanoparticles were investigated. In 2006, Ahmad et al. synthesized 3',4',5,7-tetramethoxyflavone starting from 3,4,4',6'-tetramethoxychalcone. In this transformation, SeO_2 was used as a catalyst (Ahmad, et al. 2006) shown in Figure 3.20;

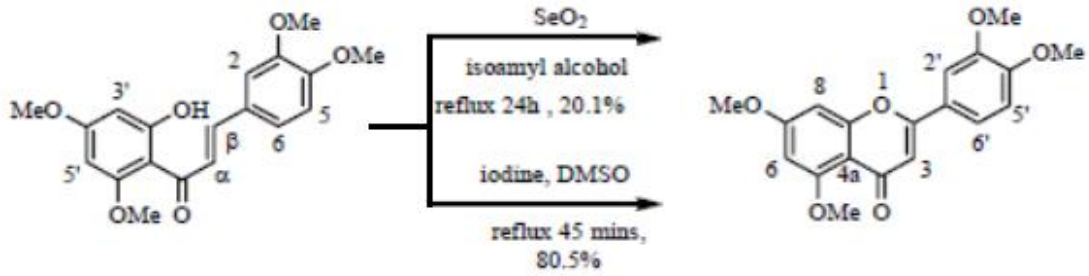

Figure 3.20. Transformation of 3,4,4',6'-tetramethoxychalcone to 3',4',5,7 tetramethoxyflavone in presence of SeO_2

A similiar catalytic study was performed according to this study by changing the catalyst from SeO_2 to CeO_2. The expected sequence of reaction is illustrated in Figure 3.21. In the firs step, a base catalyzed transformation of 2'-hydroxychalcone **(1)** into flavanone **(2)** was expected and in the second step produced flavanones will be oxidized to corresponding flavone **(3)** in the presence of CeO_2 nanoparticles. Alternatively 2'-hydroxychalcone may be converted directly into flavone **(3)**.

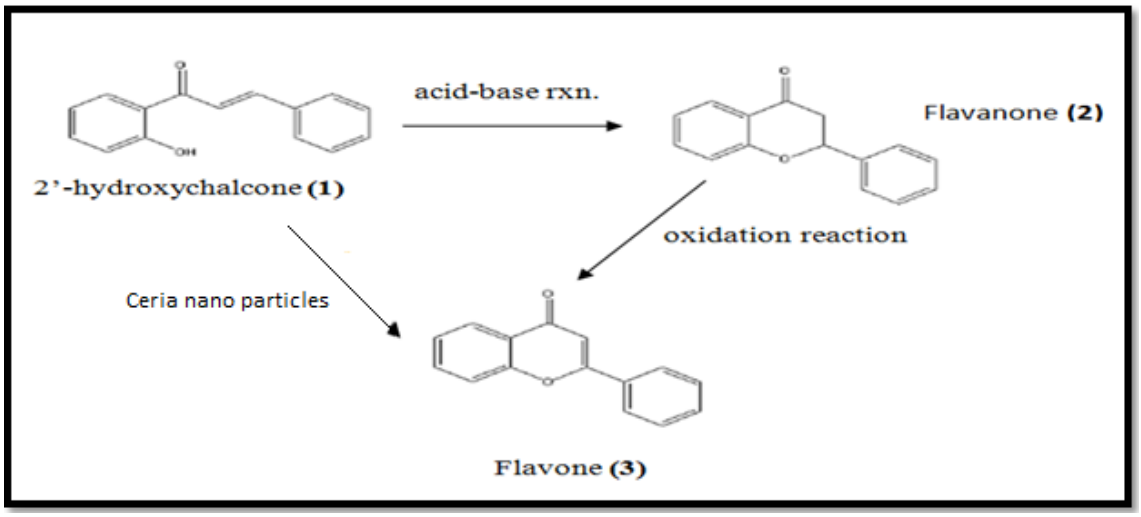

Figure 3.21. Expected synthesis routs of flavone **(3)** from 2'-hydroxychalcone **(1)**.

Calibration curves of 2'-hydroxychalcones, flavanones and flavones compared to internal standard (hexadecane) were drawn and these calibration curves were used to calculate the time dependent concentrations of the starting material and products in the

reaction mixture. Appendix A, Appendix B and Appendix C are shown the calibration curve of 2'-hydroxychalcone, flavanone and flavone respectively.

Reactions were carried out in different solvents and temperatures. Two type of ceriumoxide nanoparticles were used in the reactions. One of them is unactivated CeO_2 nanoparticles and other one is activated CeO_2 nanoparticles that were treated with 8M NaOH solutionprior to reactions. When unactivated CeO_2 nanoparticles and NaOH were used solely transformation of 2'-hydroxychalcones to flavones was unsuccesfull. However NaOH treated CeO_2 nanoparticles were catalyzed both steps in the transformation yet the yields of the product were low. In Figure 3.22, time-dependent changes in the concentrations of starting material and products were shown.

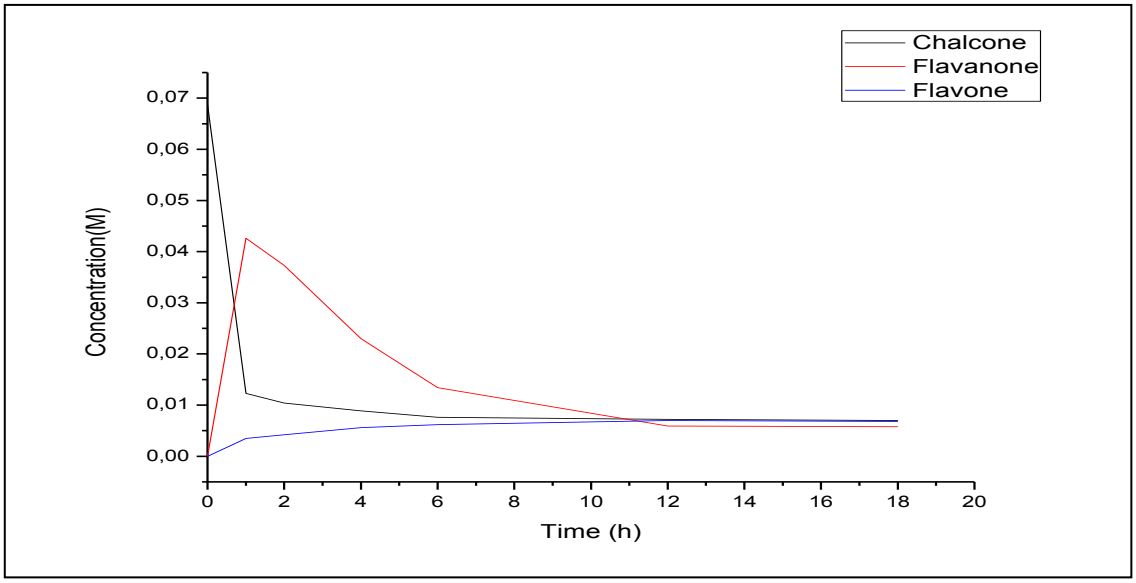

Figure 3.22. Changes in the concentrations of 2'-hydroxychalcone, flavanone and flavone catalyzed by activated CeO_2.

As it can be seen from the graph there is a net loss of material from mass balance. Somehow the amount of starting material consumed is greater than the amount of the total yields of the products. Almost 70% of the starting materials were lost according to our calibration curves.

Additionally the same reaction was carried out under the same conditions and products were isolated just to see the mass balance of the reaction. Again the amount of the starting materials was consumed and products were formed showed that there was a 45% loss of material during the reaction.

This loss of material can be originated from either by the formation of other products which are soluable in water or it can be originated from the deposition of organic molecules on CeO_2 surface.

To test the possible deposition of organic molecules, the CeO_2 particles are collected from reaction medium and washed 3 times by ethyl acetate then FTIR and SEM-EDX analysis were performed. As it can be seen from figure 3.23, IR spectrum of CeO_2 particles recovered from reaction gave two clear peak at 2928 cm^{-1} and 2864 cm^{-1} compared to the IR spectrum of activated CeO_2 particles.

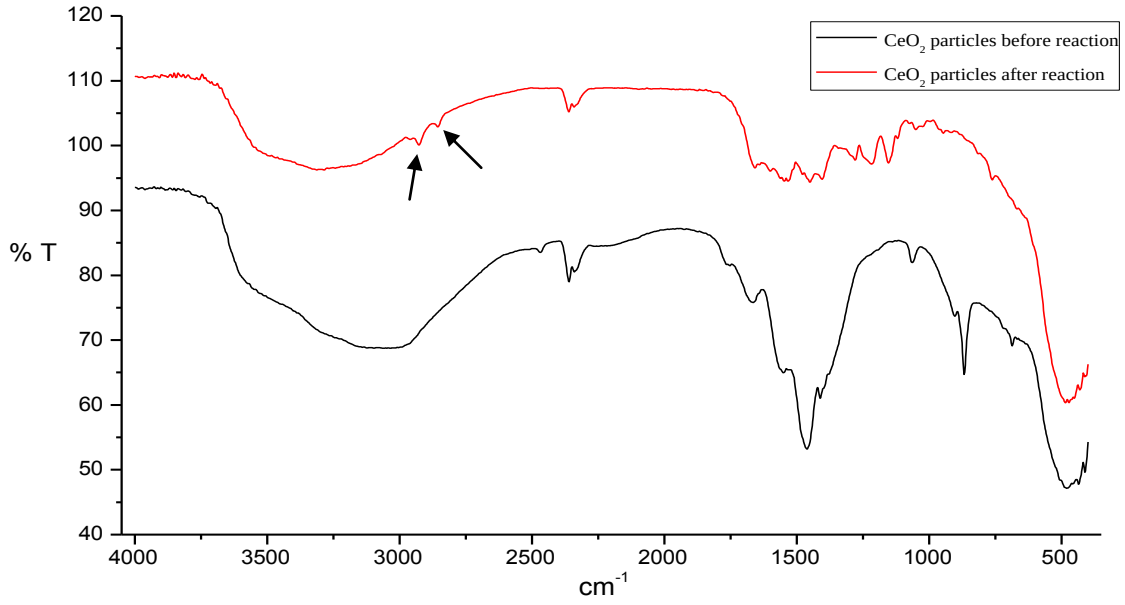

Figure 3.23. FTIR spectrum of CeO_2 particles before and after reaction.

Comparision of IR spectrum of CeO_2 particles, recovered from reactions, with the IR spectra of 2'-hydroxychalcone (Figure 3.24), flavanone (Figure 3.25) and flavone (Figure 3.26) showed that peaks at 2928 cm^{-1} and 2864 cm^{-1} are clearly matched with the peaks of 2926 cm^{-1} and 2854 cm^{-1} of flavone's IR spectrum. It seems that formed flavones are deposited on CeO_2 surface.

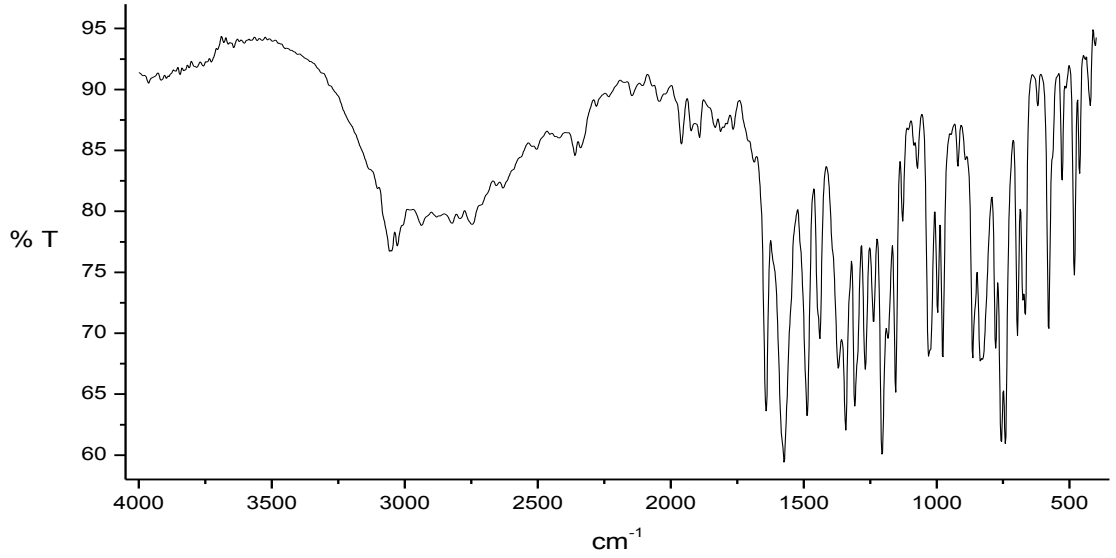

Figure 3.24. FTIR spectrum of 2'-hydroxychalcone.

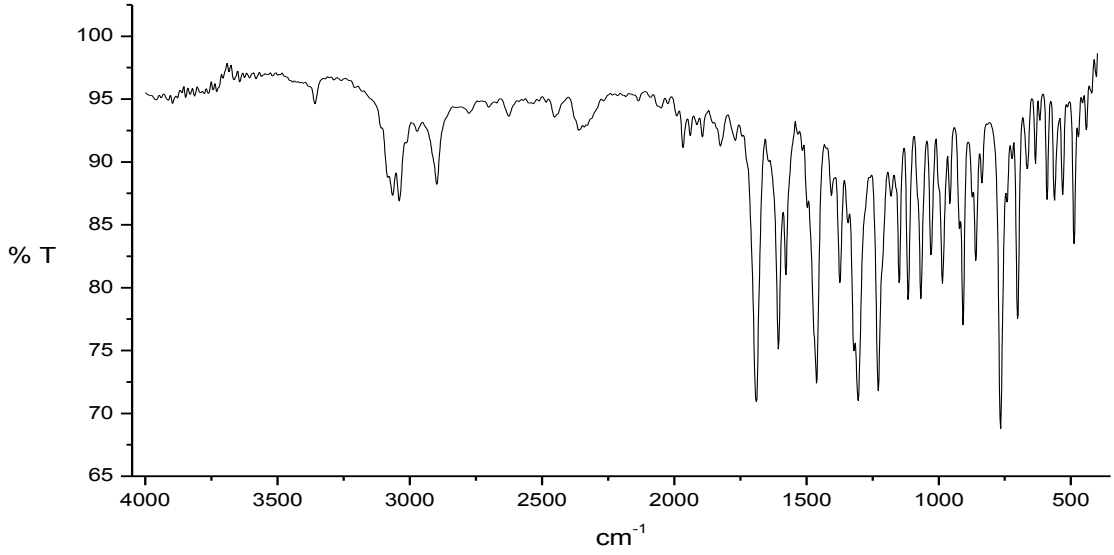

Figure 3.25. FTIR spectrum of flavanone.

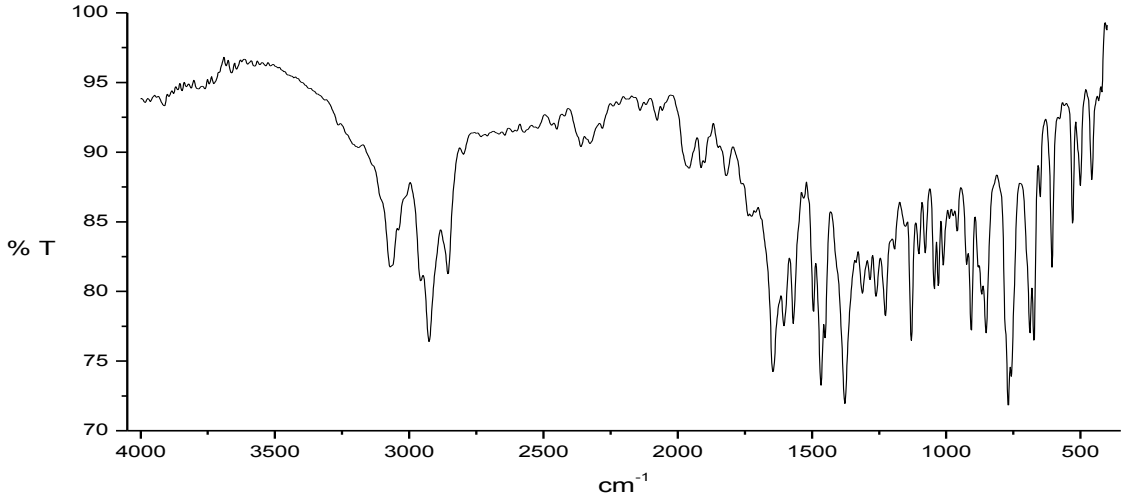

Figure 3.26. FTIR spectrum of flavone.

Deposition of product on the surface of CeO_2 nanoparticles were also checked by performing SEM-EDX mapping analysis. In Figure 3.27, EDS layered image of CeO_2 nanoparticles before reaction and in Figure 3.28, EDS layered image CeO_2 nanoparticles recovered from reactions were shown. So it can be seen that organic molecules were attached on the surface of CeO_2 nanoparticles during the reaction according to the carbon atoms were on the surface of nanoparticles.

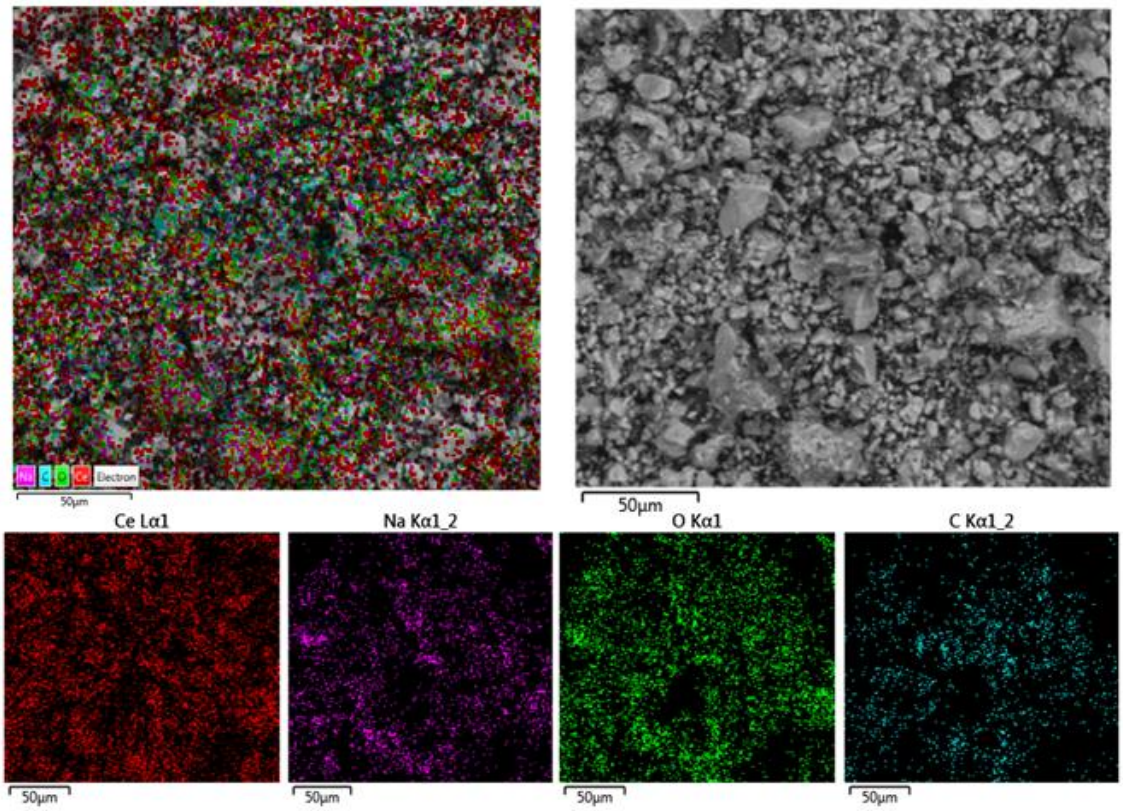

Figure 3.27. EDS layered image of CeO_2 nanoparticles before reaction.

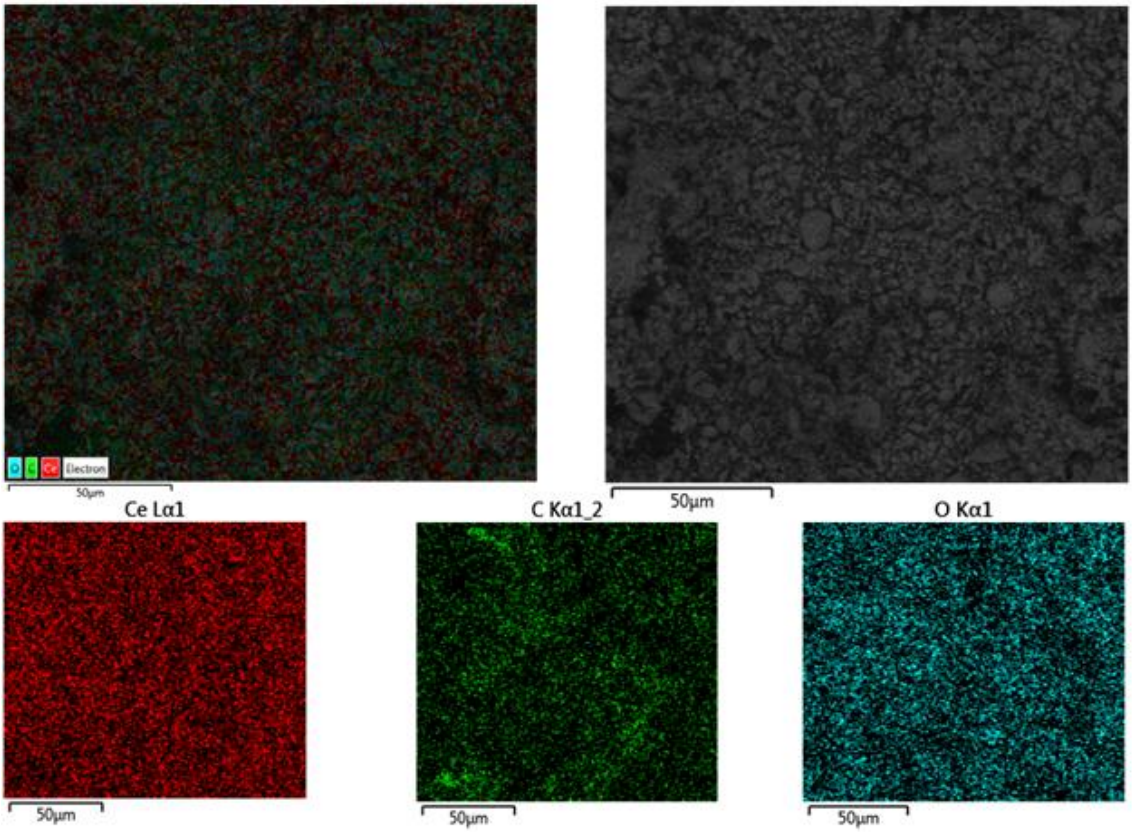

Figure 3.28. EDS layered image of CeO_2 nanoparticles after reaction.

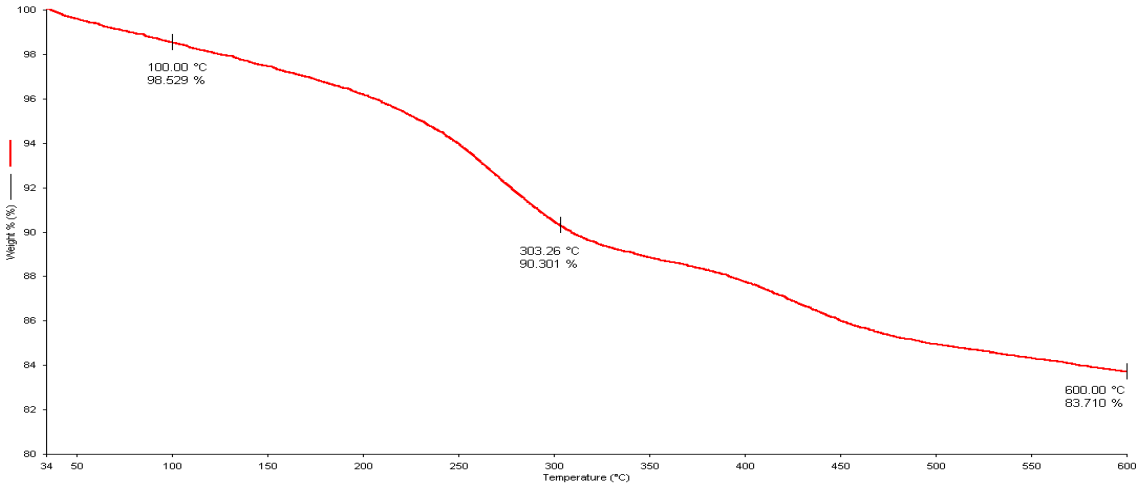

Figure 3.29. TGA graph of CeO_2 particles after reaction.

In Figure 3.29, TGA graph of CeO_2 particles after reaction were shown. There was 10% loss of material between 200°C and 450°C that refer to organic compounds. So

it can be said that according to both FTIR, SEM-EDX and TGA analysis some of the flavone deposited on the surface of the ceria particles during the reaction.

Reactions were also performed both open atmosphere and under $N_{2(g)}$ atmosphere to see any effect on the reaction yield. In both atmospheres, reaction yield was changed about 12% -15%.

Effect of solvent on reaction yield was checked by using DMSO and DMF as solvent. When the results were compared, yield of these reactions were similiar and changed between %12 and %15 according to the calibration curves. For same reactions, yield was 32% after isolated by column chromotography.

Morphologically different CeO_2 nanoparticles, rod-like and cubic, were also used to determine the effect of the shape of nanoparticles on the catalytic properties of CeO_2. Results were almost similiar so particle morphology was not a determinative parameter for flavone synthesis.

It seems that flavone formation is independent from flavanone concentration. So the overall transformation was shown in Figure 3.30.

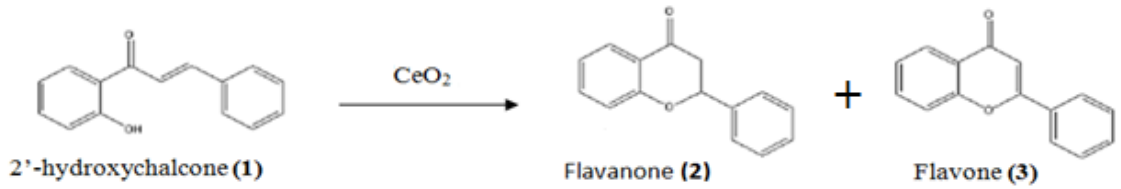

Figure 3.30. Synthesis of flavone (3) from 2'-hydroxychalcone (1).

Unactivated CeO_2 nanoparticles were also tested for the synthesis of flavone **(3)** starting from flavanone **(2)**. It was expected that flavanone is an intermediate product for the transformation of 2'-hydrocychalcone **(1)** to flavone **(3)** (Figure 3.21). When the reaction was started from flavanone **(2)** it did not yield any flavone **(3)**. Although it is just an oxidation reaction, unactivated CeO_2 nanoparticles was not able to catalyze this reaction (Figure 3.31). These results showed that flavanone **(2)** might not be a possible intermediate product for the transformation of 2'-hydrocychalcone **(1)** to flavone **(3)**.

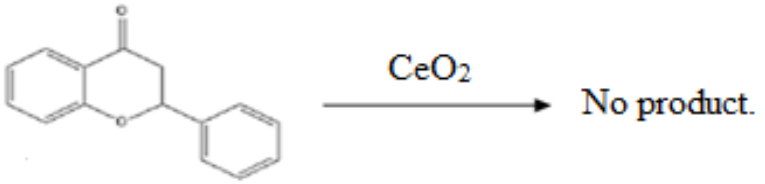

Figure 3.31. Result of the reaction of flavanone over unactivated CeO_2 nanoparticles.

Hence the flavanone may not be an intermediate, to search for possible intermediate formations a simple chalcone we subjected to react with activated CeO_2 nanoparticles. It seems that there was no reaction and α,β-unsatutared carbonyls are inactive toward activated CeO_2 nanoparticles in the absence of an intramolecular Michael reaction (Figure 3.32).

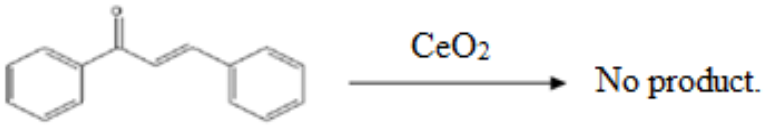

Figure 3.32. Result of the reaction of chalcone with activated CeO_2 nanoparticles.

CHAPTER 4

CONCLUSION

Cerium oxide nanoparticles were synthesized via hydrothermal method. Characterization of the synthesized cerium oxide nanoparticles was carried out by applying XRD and SEM spectroscopic methods. This study consisted of two stages. In the first stage of the study, effect of mineralizer type and concentration, surfactant, reaction temperature and reaction time on morphology and size of cerium oxide nanoparticles were investigated.

Syntheses that were performed to determine the effect of mineralizer type and the effect of surfactant were carried out using both urea and NaOH. For other parameters such as concentration, reaction temperature and reaction time, only urea was used as mineralizer. The effect of mineralizer type was clearly observed as smaller sized particles were synthesized by NaOH, about 25 nm, compared to particles that were synthesized by urea, about 125 nm. The smaller crystal sized particles were synthesized by urea, about 12 nm, compared to particles that were synthesized by NaOH, about 20 nm. While sphere-like particles were observed for NaOH, plate shape particles were seen for urea in SEM images. Additionally the effect of surfactant to particle shape and size was investigated. Different PEG types were used in these experiments and it was seen that there was not a significant change on particle sizes and shape yet a small decrease was observed for crystal size of particles that were synthesized by NaOH. Influence of concentration on particles was observed clearly. With the decreasing of concentration, both particle size and crystal size became bigger. Also morphologies of particles were changed due to concentration. For 0.1M, cubic shape particles and for 0.5 M, triangular prism shape particles were observed. For other concentration values, agglomerated spherical particles were obtained.

To see effect of reaction temperature, studies at 60^{o}C, 90^{o}C, 120^{o}C, 180^{o}C and 240^{o}C were performed. Particles that were obtained at 60^{o}C and 90^{o}C were heavily agglomerated so it was not possible to comment about particle sizes and their crystal sizes were about 10 nm. When the studies at 120^{o}C, 180^{o}C and 240^{o}C were compared, with the rising temperature agglomeration was increased so smaller particles at 120^{o}C

and bigger particles at 240^{o}C were seen. Shapes of particles for these 3 experiments were agglomerated non-unifrom sphericals. The effect of reaction time was determined using time intervals of 1h, 12h and 24h. Formation of particles was observed even for 1h synthesis and no difference on crystal size was seen. On the other hand, with the increasing reaction time decrease in particle size was observed. For 24h studies, a wide range of particle size and some cubic shape particles as well as spherical ones were observed.

In the second stage of the study, catalytic properties of CeO_2 nanoparticles synthesized using NaOH were investigated by using them as catalyst in the transformation of 2'-hydroxychalcones to flavones. Reactions were carried out with activated and unactivated ceria. Surface of the CeO_2 nanoparticles were activated by treating them 8M NaOH solution. When unactivated CeO_2 nanoparticles and NaOH were used solely transformation of 2'-hydroxychalcones to flavones was unsuccesfull. However desired product was synthesized by using activated CeO_2 nanoparticles yet the yields of the products were low. Net loss of materials was observed from the GC-MS analysis of samples taken from reaction mixture and calibration curves.

Two possible scenarios are proposed for the loss of materials. First one is the formation of side products which are soluble in water and the second one is deposition of organic molecules on the CeO_2 surface. FTIR, TGA and SEM-EDX analysis of CeO_2 nanoparticles used in the reaction were used to test the second case and the depositions of organic molecules were determined on the surface of CeO_2 nanoparticles.

Total yield of flavone was determined as 42.5% by adding loss of materials amount in TGA to isolated flavone amount by column chromatography.

Different solvents were tried to obtain any effect on reaction yield originated by solvents yet no difference on yield was obtained. Yields of both trials were changed between %12 and % 15 that were calculated by calibration curves.

Rod-like and cubic shape activated CeO_2 nanoparticles were tried in transformation of 2'-hydroxychalcones to flavones to see any effect of the shape of CeO_2 nanoparticles on catalytic activity and it can be said that particle morphology is not a determinative parameter.

REFERENCES

Ahmad, F., Idrıs, M.S.H, Adıb, A.B. 2006. Synthesis and characterization some flavanoids derivatives. Department of Chemistry Faculty of Science. Universiti Teknologi Malaysia. Unpublished.

Arts, I. C. W. and Hollman, P. C. H. 2005. Polyphenols and disease risk in epidemiologic studies. *American Journal of Clinical Nutrition.* 1:317-325.

Bera, P., A. Gayen, M. S. Hegde, N. P. Lalla, L. Spadaro, F. Frusteri, and F. Arena. 2003. Promoting effect of CeO2 in combustion synthesized Pt/CeO_2 catalyst for CO oxidation. *Journal of Physical Chemistry.* 25:6122-6130.

Bohm, J. 1975. A. N. Lobachev (Herausgeber). Crystallisation processes under hydrothermal conditions. Consultants Bureau, Plenum Publishing Corp., New York – London 1973; 255 Seiten, zahlreiche Abbildungen und Tabellen. *Kristall und Technik.* 4:K56-K57.

Byrappa, K., and Yoshimura, M. 2008. *Handbook of Hydrothermal Technology*: Elsevier Science.

Byrappa, K. and Adschiri, T. 2007. Hydrothermal technology for nanotechnology. *Progress in Crystal Growth and Characterization of Materials*. 53:117-166.

Calvino, V., Picallo, M., López-Peinado, A. J., Martín-Aranda, R. M. and Durán-Valle, C. J. 2006. Ultrasound Accelerated Claisen–Schmidt Condensation: A Green Route to Chalcones. *Applied Surface Science.* 17:6071-74.

Cao, Guohong. 2004. *Nanostructures and Nanomaterials*. Singapore: World Scientific Publishing Company.

Cullity, B.D. 1956. *Elements of X-ray diffraction*: Addison-Wesley Pub. Co.

Dyke, S. F., Ollis, W. D. and Sainsbury, M. 1961. Synthesis of Isoflavones. Part III.1 Caviunin. *The Journal of Organic Chemistry.* 7:2453-2455.

Destree, C., George, S., Champagne, B., Guillaume, M., Ghijsen, J. and Nagy, J. B. 2008. J-complexes of retinol formed within the nanoparticles prepared from microemulsions. *Colloid and Polymer Science.* 1:15-30.

Dimmock, J. R., Elias, D. W., Beazely, M. A. and Kandepu, N. M. 1999. Bioactivities of chalcones. *Current Medicinal Chemistry.* 12:1125-1149.

Eastoe, J., Hollamby, M. J. and Hudson, L. 2006. Recent Advances in Nanoparticle Synthesis with Reversed Micelles. *Adv Colloid Interface Sci.* 128-130 5-15.

Go, M. L., Wu, X. and Liu, X. L. 2005. Chalcones: An update on cytotoxic and chemoprotective properties. *Current Medicinal Chemistry.* 4:483-499.

Gormley, T. R. and Osulliva, W. 1973. FLAVANOID EPOXIDES. ACID AND BASE CATALYZED REACTIONS OF 2'-TOSYLOXYCHALCONE EPOXIDES–MECHANISM OF ALGAR-FLYNN-OYAMADA REACTION.*Tetrahedron.* 2:369-373.

Goubin, F., Rocquefelte, X., Whangbo, M. H., Montardi, Y., Brec, R. and Jobic, S. 2004. Experimental and theoretical characterization of the optical properties of CeO_2, $SrCeO_3$, and Sr_2CeO_4 containina Ce^{4+} (f(0)) ions. *Chemistry of Materials.* 4:662-69.

Havsteen, B. H. 2002. The biochemistry and medical significance of the flavonoids. *Pharmacology & Therapeutics.* 2-3:67-202.

Higgins, R. J. 1997. An economical process for manufacturing of nano-sized powders based on microemulsion-mediated synthesis. In *Proc. of the Joint NSF-NIST Conf. on Nanoparticles.*

Hirano, M. And Kato, E. 1999. Hydrothermal synthesis of nanocrystalline cerium oxide powders. *J.Am. Ceram. Soc.* 82:786-788.

Jacobs, G., L. Williams, U. Graham, D. Sparks, and Davis, B. H. 2003. Low-temperature water-gas shift: In-situ DRIFTS - Reaction study of a Pt/CeO_2 catalyst for fuel cell reformer applications. *Journal of Physical Chemistry.* 38:10398-10404.

Jarvill-Taylor, K. J., Anderson, R. A. and Graves, D. J. 2001. A Hydroxychalcone Derived from Cinnamon Functions as a Mimetic for Insulin in 3t3-L1 Adipocytes. *J Am Coll Nutr.* 20:327-36.

Jasinski, P., Suzuki, T. and Anderson, H. U. 2003. Nanocrystalline undoped ceria oxygen sensor. *Sensors and Actuators B-Chemical.* 1-3:73-77.

Kang, S. J. L. 2004. *Sintering: Densification, Grain Growth and Microstructure*: Elsevier Science.

Karthikeyan, M. S., Holla, B. S. and Kumari, N. S. 2007. Synthesis and antimicrobial studies on novel chloro-fluorine containing hydroxy pyrazolines. *European Journal of Medicinal Chemistry.* 1:30-36.

Komarneni, S. 2003. Nanophase materials by hydrothermal, microwave-hydrothermal and microwave-solvothermal methods. *Current Science.* 12:1730-1734.

Kreher, U. P., Rosamilia, A. E., Raston, C. L., Scott, J. L. and Strauss, C. R. 2003. Direct preparation of monoarylidene derivatives of aldehydes and enolizable ketones with DIMCARB. *Organic Letters.* 17:3107-3110.

Laudise, R. A. 1970. *The Growth of Single Crystals*. Prentice Hall: Englewood Cliffs, NJ.

Laudise, R. A. 1987. HYDROTHERMAL SYNTHESIS OF CRYSTALS. *Chemical & Engineering News.* 39:30-&.

Li, R. X., Yabe, S., Yamashita, M., Momose, S., Yoshida, S., Yin, S. and Sato, T. 2002. Synthesis and UV-shielding properties of ZnO- and CaO-doped CeO_2 via soft solution chemical process. *Solid State Ionics*. 1-4:235-241.

Martens, S., and Mithofer, A. 2005. Flavones and flavone synthases. *Phytochemistry*. 20:2399-2407.

Miao, J. J., Wang, H., Li, Y. R., Zhu, J. M.,and Zhu, J. J. 2005. Ultrasonic-induced synthesis of CeO_2 nanotubes. *Journal of Crystal Growth.* 2-4:525-529.

Middleton, E., Kandaswami, C. and Theoharides, T. C. 2000. The effects of plant flavonoids on mammalian cells: Implications for inflammation, heart disease, and cancer. *Pharmacological Reviews.* 4:673-751.

Nowakowska, Z., Kedzia, B. and Schroeder, G. 2008. Synthesis, physicochemical properties and antimicrobial evaluation of new (E)-chalcones. *European Journal of Medicinal Chemistry.* 4:707-713.

Ou, Z. M., Yao, H. and Kimura, K. 2007. Preparation and optical properties of organic nanoparticles of porphyrin without self-aggregation. *Journal of Photochemistry and Photobiology a-Chemistry*. 1:7-14.

Platz, G. 1991. M. P. Pileni (Ed.): Structure and Reactivity in Reverse Micelles, Elsevier, Amsterdam 1989. 379 Seiten, Preis: DM 285,–. *Berichte der Bunsengesellschaft für physikalische Chemie.* 1:103-104.

Phoka, S., Laokul, P., Swatsitang, E., Promarak, V., Seraphin, S. and Maensiri, S. 2009. Synthesis, structural and optical properties of CeO_2 nanoparticles synthesized by a simple polyvinyl pyrrolidone (PVP) solution route. *Materials Chemistry and Physics.* 1:423-428.

Qi, R. J., Zhu, Y. J., Cheng, G. F. and Huang, Y. H. 2005. Sonochemical synthesis of single-crystalline $CeOHCO_3$ rods and their thermal conversion to CeO_2 rods. *Nanotechnology.* 11:2502-2506.

Rabenau, A. 1985. THE ROLE OF HYDROTHERMAL SYNTHESIS IN PREPARATIVE CHEMISTRY. *Angewandte Chemie-International Edition in English.* 12:1026-1040.

Ross, J. A., and Kasum, C. M. 2002. Dietary flavonoids: Bioavailability, metabolic effects, and safety. *Annual Review of Nutrition.* 22:19-34.

Roy, R. 1994. Accelerating the Kinetics of Low-Temperature Inorganic Syntheses. *Journal of Solid State Chemistry.* 1:11-17.

Shchukin, D. G. and Caruso, R. A. 2004. Template synthesis and photocatalytic properties of porous metal oxide spheres formed by nanoparticle infiltration. *Chemistry of Materials.* 11:2287-2292.

Skoog, D. A., Holler, F. J. and Crouch, S. R. 2007. *Principles of Instrumental Analysis*: Thomson Brooks/Cole.

Smart, L. E., and Moore, E. A. 2005. *Solid State Chemistry: An Introduction, Third Edition*: Taylor & Francis.

Sohlberg, K., Pantelides, S. T. and Pennycook, S. J. 2001. Interactions of hydrogen with CeO_2. *Journal of the American Chemical Society.* 27:6609-6611.

Strobel, H. A., and Heineman, W. R. 1989. *Chemical instrumentation: a systematic approach*: Wiley.

Suslick, K. S., Hyeon, T. W. and Fang, M. M. 1996. Nanostructured materials generated by high-intensity ultrasound: Sonochemical synthesis and catalytic studies. *Chemistry of Materials.* 8:2172-2179.

Tabak, C., Arts, I. C. W., Smit, H. A., Heederik, D. and Kromhout, D. 2001. Chronic obstructive pulmonary disease and intake of catechins, flavonols, and flavones - the MORGEN Study. *American Journal of Respiratory and Critical Care Medicine.* 1:61-64.

Tanaka, John, and Suib, S. L. 1999. *Experimental Methods in Inorganic Chemistry*: Prentice Hall PTR.

Tok, A. I. Y., Boey, F. Y. C., Dong, Z. and Sun, X. L. 2007. Hydrothennal synthesis of CeO_2 nano-particles. *Journal of Materials Processing Technology.* 1-3:217-222.

Wang, C. H. and Lin, S. S. 2004. Preparing an active cerium oxide catalyst for the catalytic incineration of aromatic hydrocarbons. *Applied Catalysis a-General.* 1-2:227-233.

Winsor, P. A. 1948. Hydrotropy, Solubilisation and Related Emulsification Processes. *Transactions of the Faraday Society.* 0:376-98.

Yarishkin, O. V., Ryu, H. W., Park, J. Y., Yang, M. S., Hong, S. G. and Park, K. H. 2008. Sulfonate chalcone as new class voltage-dependent K^+ channel blocker. *Bioorganic & Medicinal Chemistry Letters.* 1:137-140.

Yin, L. X., Wang, Y. Q., Pang, G. S., Koltypin, Y. and Gedanken, A. 2002. Sonochemical synthesis of cerium oxide nanoparticles - Effect of additives and quantum size effect. *Journal of Colloid and Interface Science.* 1:78-84.

Zhang, W. Z., Qiao, X. L. and Chen, J. G. 2006. Synthesis and characterization of silver nanoparticles in AOT microemulsion system. *Chemical Physics.* 3:495-500.

APPENDIX A

CALIBRATION CURVE OF 2'-HYDROXYCHALCONE

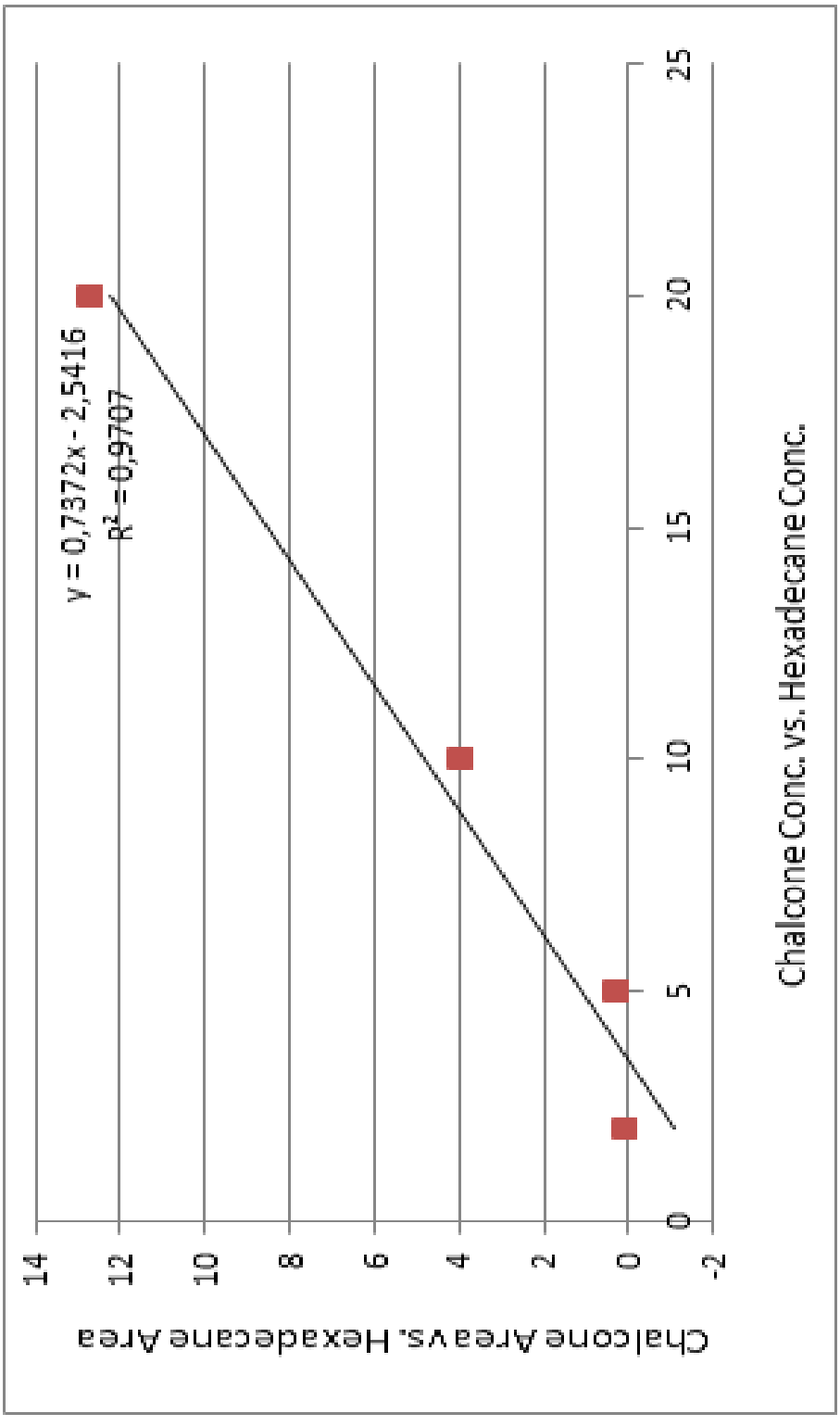

Figure A.1. Calibration Curve of 2'-Hydroxychalcone

APPENDIX B

CALIBRATION CURVE OF FLAVANONE

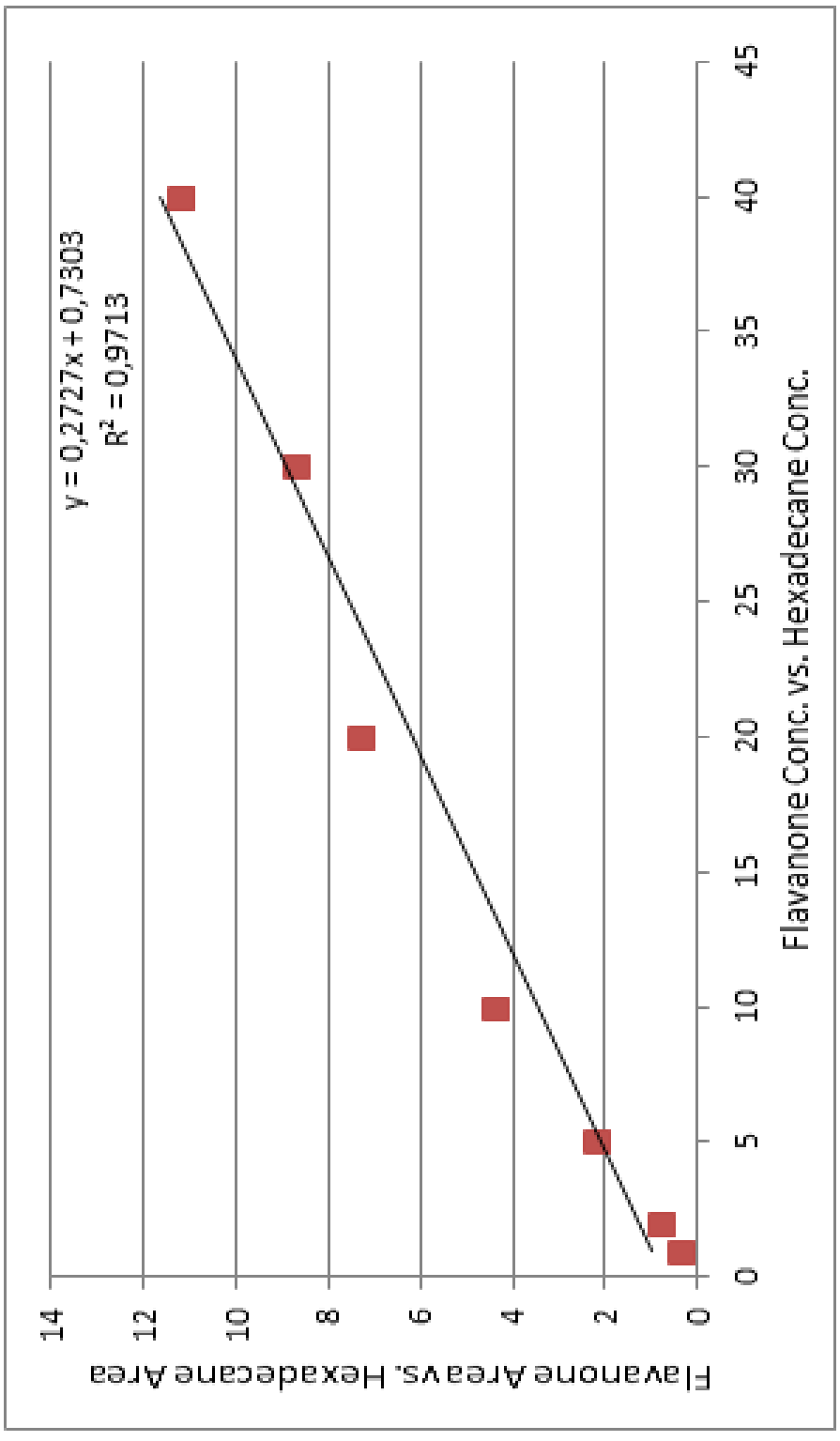

Figure B.1. Calibration Curve of Flavanone

APPENDIX C

CALIBRATION CURVE OF FLAVONE

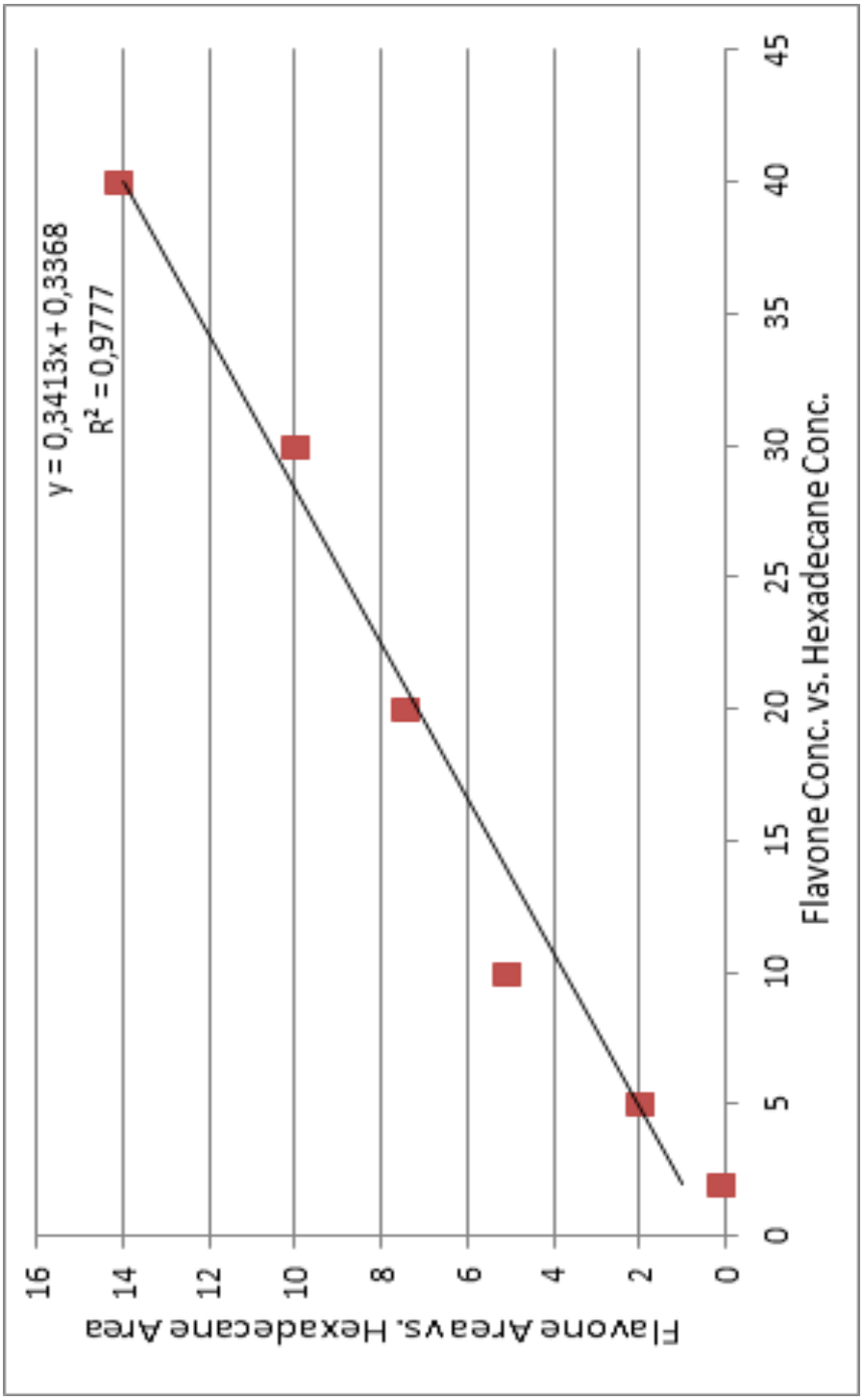

Figure C.1. Calibration Curve of Flavone

APPENDIX D

EDX SPECTRUM OF CeO_2 PARTICLES AFTER REACTION

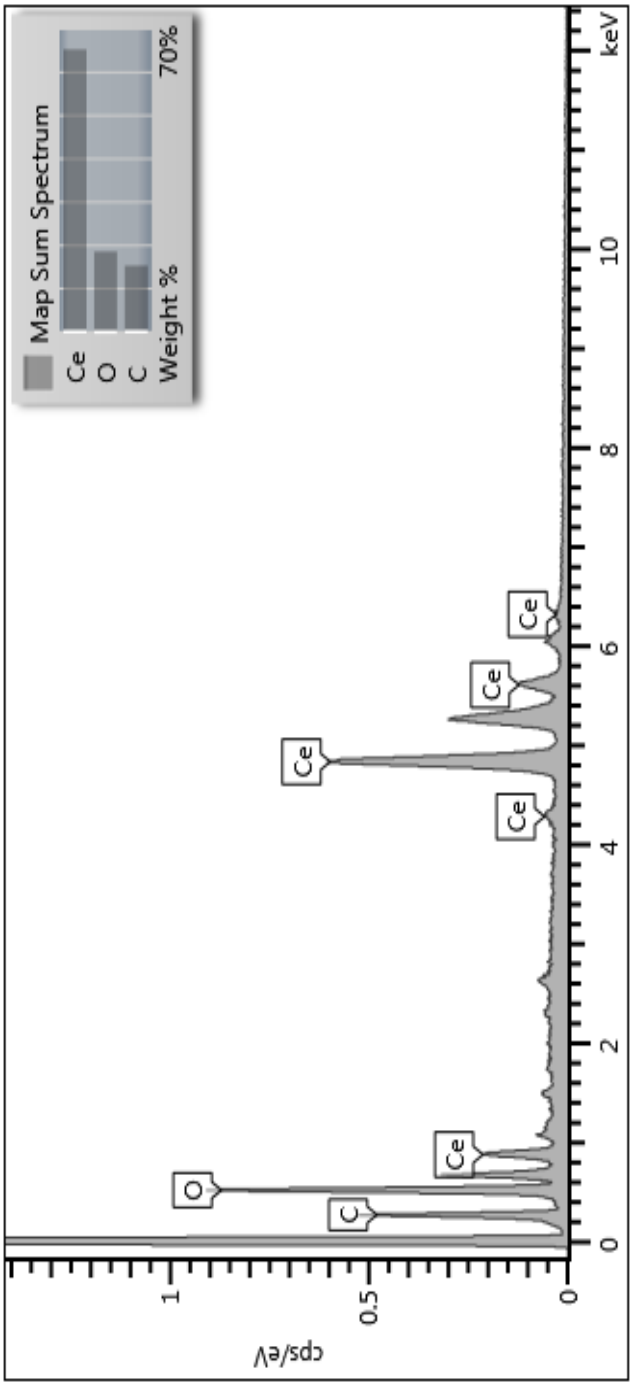

Element	Wt%	Atomic %
C	15.61	44.12
O	18.85	40.00
Ce	65.54	15.88
Total:	100.00	100.00

Figure D.1. Percentages of elements that were contained in the after reaction CeO_2 particles

APPENDIX E

GC-MS SPECTRUM OF FLAVANONE

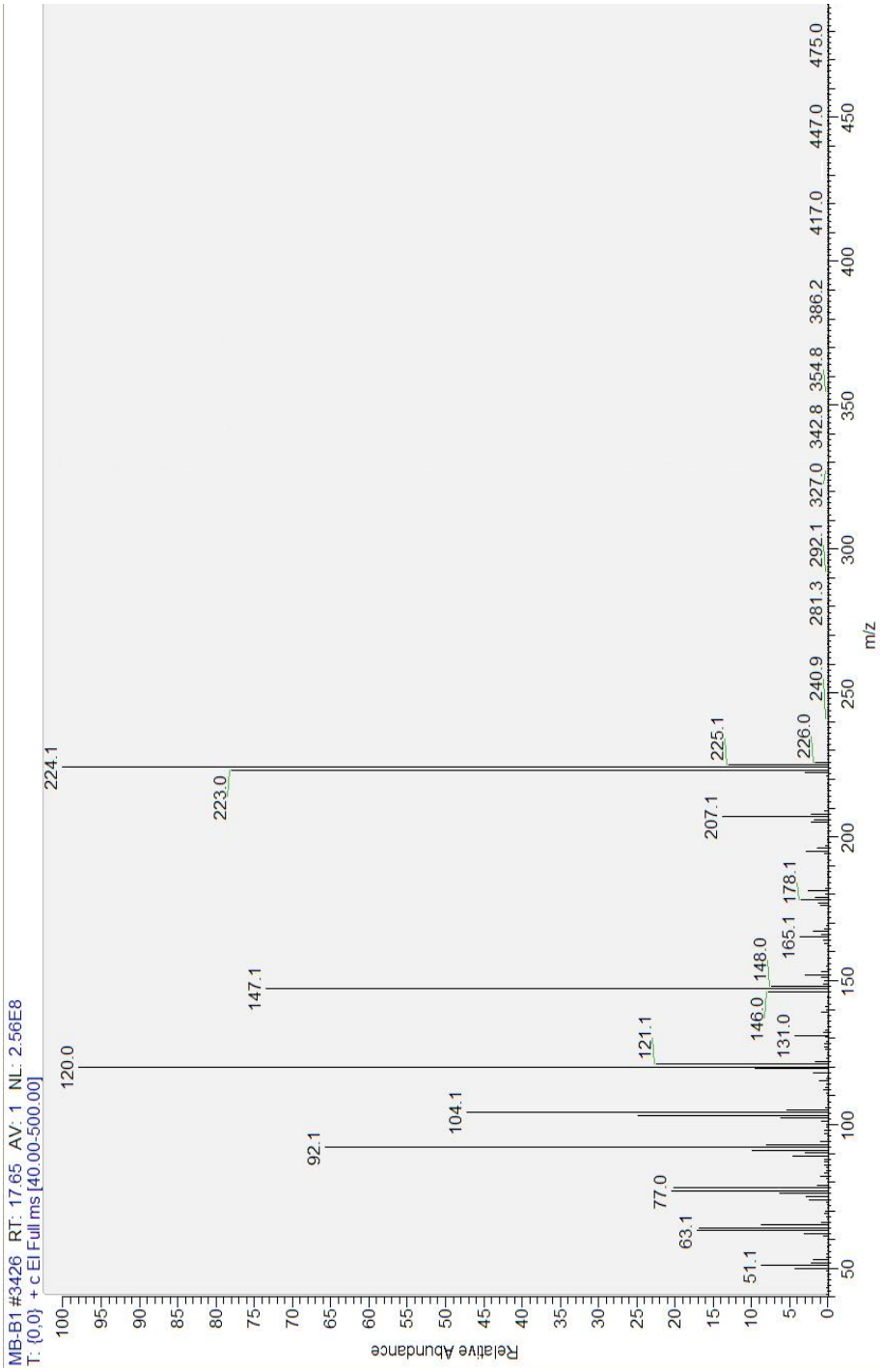

Figure E.1. MS Spectrum of Flavanone

APPENDIX F

GC-MS SPECTRUM OF FLAVONE

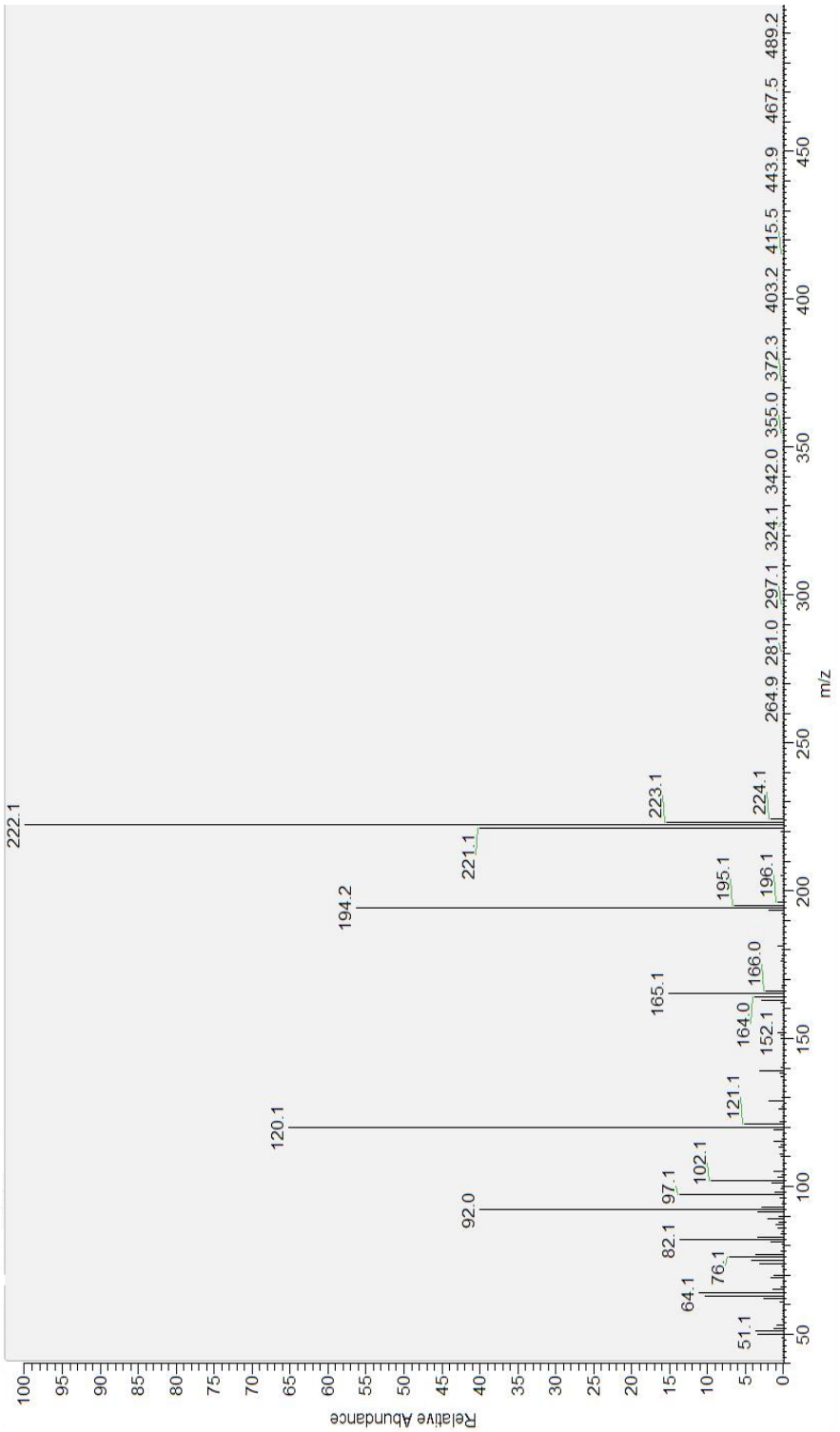

Figure F.1. MS Spectrum of Flavone

APPENDIX G

^{1}H NMR SPECTRUM OF FLAVANONE

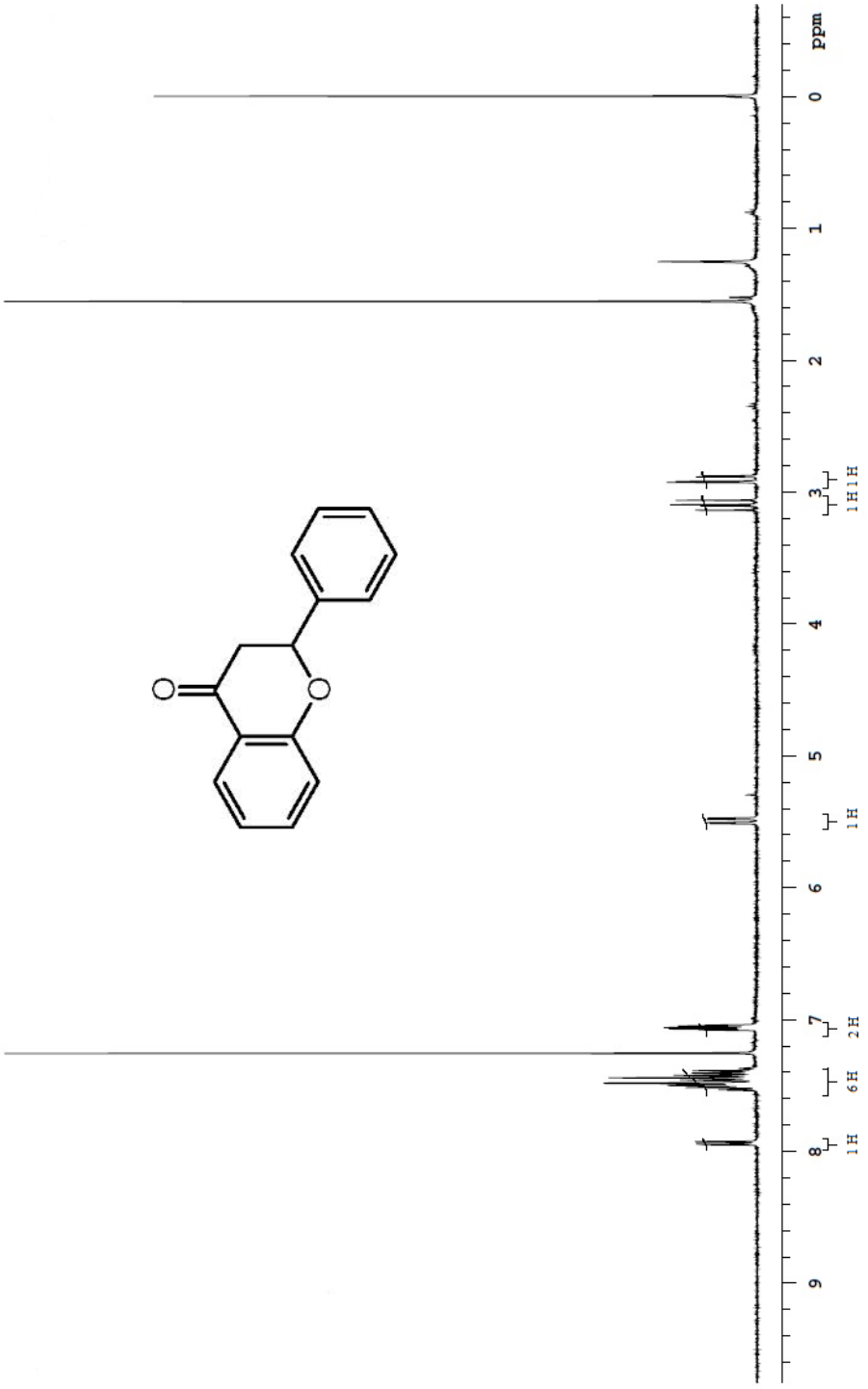

Figure G.1. ^{1}H NMR Spectrum of Flavanone

APPENDIX H

^{1}H NMR SPECTRUM OF FLAVONE

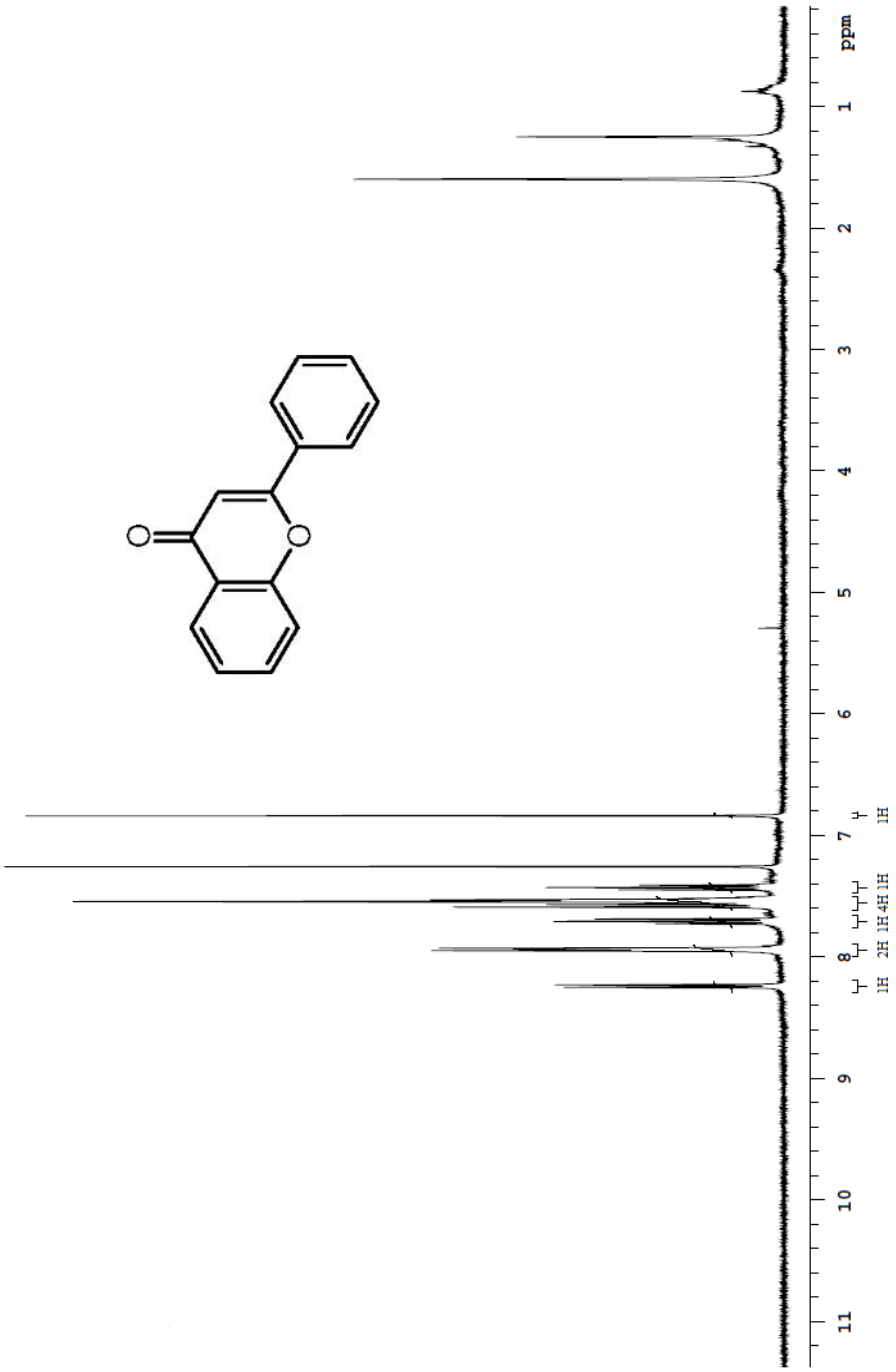

Figure G.1. ^{1}H NMR Spectrum of Flavone